PETROLOGY AND CRYSTAL CHEMISTRY OF THE RUBY STAR GRANODIORITE PIMA COUNTY, ARIZONA

by

Nancy Jane Hess

A Thesis Submitted to the Faculty of the

DEPARTMENT OF GEOSCIENCES

In Partial Fulfillment of the Requirements
For the Degree of

MASTER OF SCIENCE

In the Graduate College

THE UNIVERSITY OF ARIZONA

1 9 8 6

STATEMENT BY AUTHOR

This thesis has been submitted in partial fulfillment fo requirements for an advanced degree at the University of Arizona and is deposited in the University Library to be made available to borrows under the rules of the Library.

Brief quotations from this thesis are allowable without special permission, provided that accurate acknowledgment of source is made. Requests for permission for extended quotation from or reproduction of this manuscript in whole or in part may be granted by the head of the major department of the Dean of the Graduate College when in his or her judgment the proposed use of the material is in the interests of scholarship. In all other instances, however, permission must be obtained from the author.

SIGNED: _____nancyhen_____

APPROVAL BY THESIS DIRECTOR

This thesis has been approved on the date shown below:

_____ _____April 29, 1986_____

S. R. Titley, Professor Date

ACKNOWLEDGMENTS

This study was made possible by the use of the SEMQ facilities in the Lunar and Planetary Sciences Department at the University of Arizona under the guidence of Tom Teska. I am very gratiful to M. Darby Dyar and Kurt Fredrikson for perfoming the ferrous-ferric determinations of biotite, to Libby Anthony and Spencer Titley, my adviser, for their encouragement and advice, and to my committee members, Jibamitra Ganguly and Joaquin Ruiz, for their reviews of this manuscript.

This study was funded by National Science Foundation Grant EAR 8218875 to Dr. Titley.

TABLE OF CONTENTS

TABLE OF CONTENTS - - CONTINUED

LIST OF ILLUSTRATIONS

LIST OF ILLUSTRATIONS -- CONTINUED

LIST OF TABLES

ABSTRACT

The Laramide-aged Ruby Star batholith consists of an outer equigranular granodiorite rim and an inner porphyritic granodiorite core. A quartz monzonite stock breaches the southern rim of the batholith and together with the discontinuous bodies of biotite quartz diorite host the Sierrita-Esperanza porphyry copper deposit.

The whole rock data indicate that the granodiorite crystallized at 650 to 700 C and a fH_2O of 1800 to 2000 bars. Analyses of biotite show Mg enrichment in biotite with simultaneous Fe enrichment in the host rock. These trends and the presence of magnetite suggest that Ruby Star batholith crystallized at high and increasing fO_2. The biotite dehydration reaction of Czamanske and Wones (1973) suggests that crystallization occurred at fO_2 of 10^{-14} to 10^{-16} bars at 750 to 650 C. These temperature-fO_2 conditions match those required for hydrothermal fluids to carry sulphur species that complex copper (Burnham and Ohmoto, 1980).

CHAPTER 1

INTRODUCTION

Geologic Setting

The Laramide-aged Ruby Star Granodiorite crops out low on the northern portions and the eastern flank of the Sierrita Mountains as a roughly oval-shaped batholith (see Figure 1). The batholith intrudes intensely folded and faulted Mesozoic and Paleozoic-aged volcanic and volcaniclastic rocks on its southern and western edges, and intrudes or is in thrust contact with late Paleozoic sedimentary rocks on its eastern edge. Much of the eastern and northern contacts of the batholith with older rocks is covered by Cenozoic volcanic rocks and alluvium. The Paleozoic section consists predominately of carbonate and sandstone units. The Mesozoic volcanic section consists of andesite and welded, vitreous dacitic to rhyolitic tuffs. The Ruby Star Granodiorite has been radiometrically dated at 58.7 to 61.6 million years (Damon, 1966; Cooper, 1971).

The Granodiorite is concentrically zoned consisting of a hornblende-titanite-biotite bearing equigranular rim and a titanite-biotite bearing porphyritic interior. Just south of the batholith are small, elongate bodies of biotite

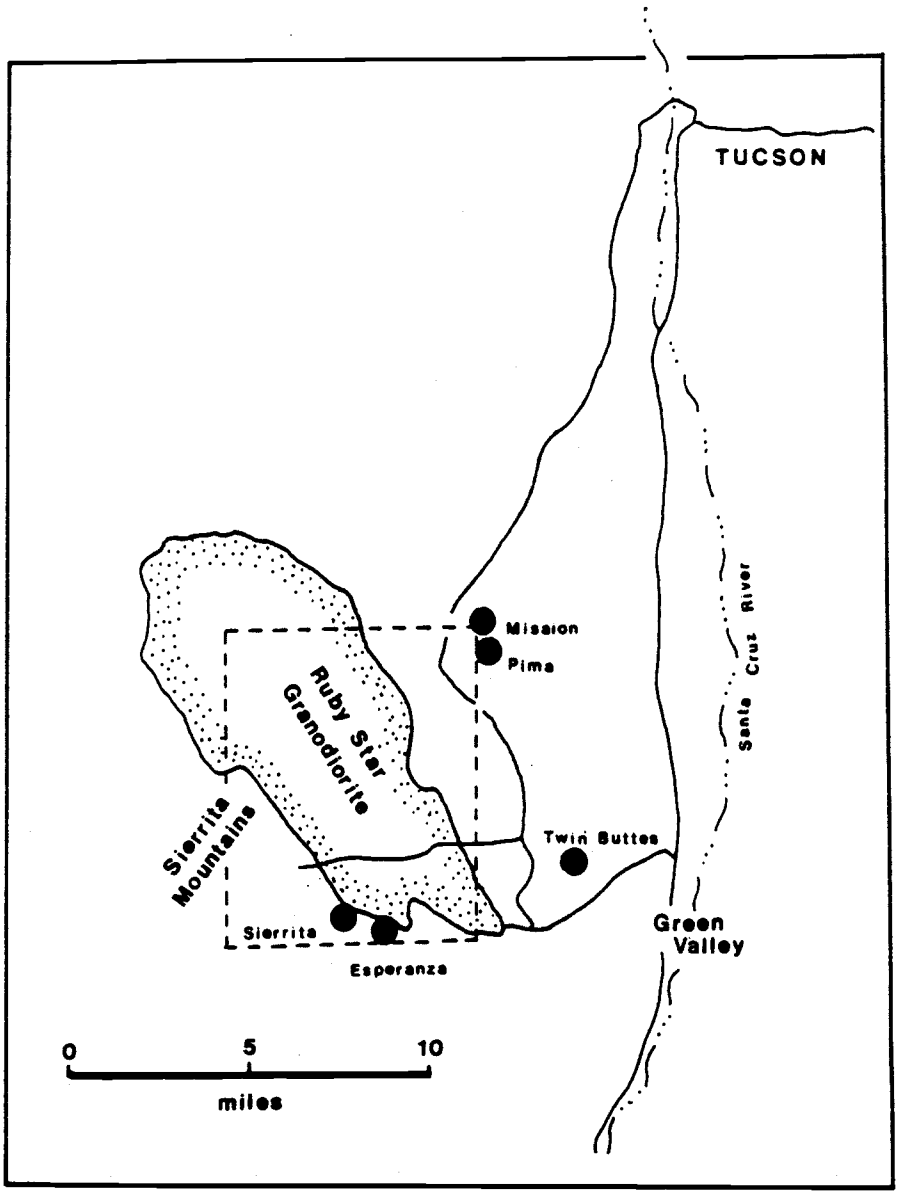

Figure 1. Location Map of Field Area.

The roughly oval-shaped body aligned to the northwest is the Ruby Star Granodiorite located within the Pima Mining District. The circles are porphyry copper deposits within the district. The area within the small rectangle is enlarged in Figure 2. (Modified after Mauger, 1966).

quartz diorite that crop out in a discontinuous string aligned to the northwest some of which are enclosed in the Granodiorite. The biotite quartz diorite has been radiometrically dated at 67 million years (Cooper, 1973). The relationship between the biotite quartz diorite and the Granodiorite is problematical. Sm-Nd isotopic ratios indicate that the Granodiorite and the biotite quartz diorite are not related by a simple fractional crystallization history (Anthony, 1986). At the south edge of the batholith bodies of porphyritic quartz monzonite breach the equigranular rim and together with the biotite quartz diorite host porphyry copper mineralization (see Figure 2).

For the purposes of this investigation, the Granodiorite has been separated into two members: the equigranular rim and the porphyritic core. The equigranular rim member has been further subdivided into the eastern, western, and southern rim. The members are distinguished on the basis of texture and minor and accessory modal mineralogy, whereas the subdivision of the equigranular rim is geographical. The biotite quartz diorite has been included in this study because of its importance as a host to porphyry copper mineralization although its genetic relationship to the Granodiorite remains unclear. Samples of the mineralized quartz monzonite porphyry were not analyzed because fresh samples were not found.

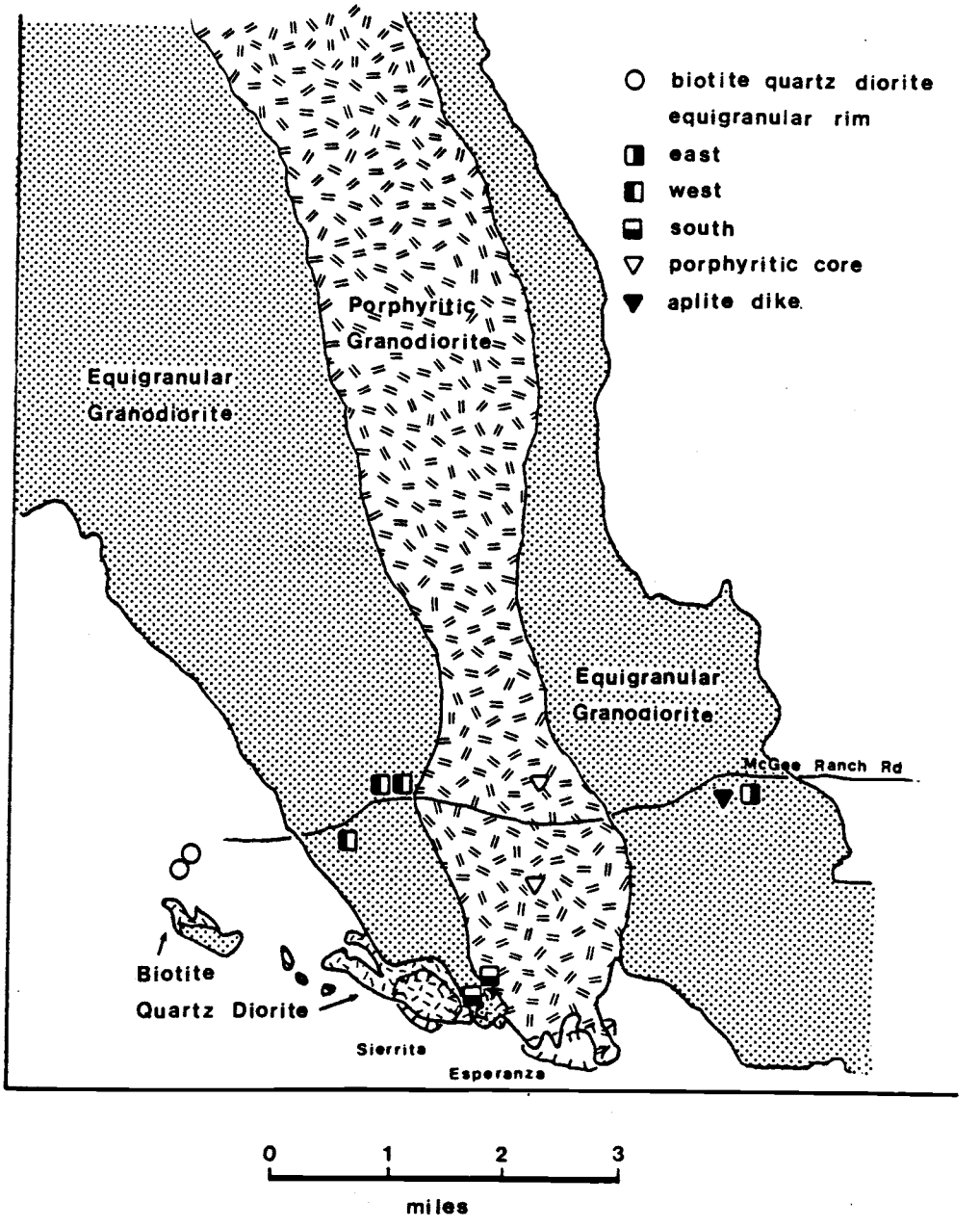

Figure 2. Sample Location Map.

Generalized map of the distribution of the biotite-quartz diorite and the granodiorite equigranular rim and porphyry core phases. The circles indicate sample locations (After Lovering et al., 1970).

Purpose

Although the geology and many of the characteristics of the porphyry copper mineralization at Sierrita are well known, no work has been done to determine the intensive variables prevailing during the crystallization of the Ruby Star Granodiorite. This study uses the variation in biotite crystal chemistry as an indicator of changing oxygen fugacity, temperature and partial pressure of water.

Whether oxygen fugacity increases, stays the same, or decreases during differentiation has important implications to the development of a vapor phase during crystallization and its subsequent role as an oxygen fugacity buffer (Mueller, 1969; Mueller and Saxena, 1977). A change in oxygen fugacity during crystallization could be a significant control in the genesis of porphyry copper deposits (Burnham and Ohmoto, 1982).

Previous Work

The general geology and stratigraphy of the Sierrita Mountains were first described by Ransome (1922). The petrography and their structural significance of the granodiorite has been described by Cooper (1960). Cooper described in detail the petrography of the Mesozoic volcanic section within the Sierrita Mountains (Cooper, 1971).

Lovering (1970) has studied the copper content of biotites from intrusive rocks genetically related to porphyry copper mineralization within the Pima District in the Sierrita Mountains and nearby porphyry copper mineralization in the Santa Rita Mountains.

The geologic setting and the economic geology of the Sierrita-Esperanza, Twin Buttes, and Mission porphyry copper mines as well as the tectonic history of the Pima Mining District as a whole has been well established (Titley, 1982; West and Aiken, 1982). Most recently, the Sierrita-Esperanza deposit has been the site of a detailed fracture study and the relationship of the fractures to mineralization (Titley et al, 1986).

Based on a trace element study of the Late Mesozoic igneous units Anthony (1986) suggests that the 59 to 62 m.y. old Ruby Star Granodiorite and the overlying 68 m.y. old Demetrie Andesite and 65 to 70 m.y. old Red Boy Rhyolite can be interpreted as representing a co-magmatic suite. Following Anthony's model, the parent magma was generated from a crustal source and the Andesite, Granodiorite, and Rhyolite are related by process that includes both fractional crystallization and assimilation (Anthony, 1986).

CHAPTER 2

PETROGRAPHY

Modal analyses of the Ruby Star Granodiorite and the biotite quartz diorite are compiled in Table 1. A summary of the relevant petrographic characteristics is given below.

Petrographic Descriptions

Biotite-Quartz Diorite

The biotite-quartz diorite is fine-grained and slightly porphyritic. Moderately zoned, 1 to 3mm plagioclase laths are set in a mosaic of 0.1 to 0.3mm grains of subhedral plagioclase, quartz, anhedral potassium feldspar, and aggregates of fine-grained biotite and clinopyroxene. Biotite occurs predominately as abundant, fine-grained aggregates, possibly of secondary origin, and rarely as large, optically continuous flakes surrounding clinopyroxene fragments. Some fine-grained biotite aggregates form elongate clusters that psuedomorph clinopyroxene and contain abundant magnetite. A few of the smaller biotite flakes are replaced by trace amounts of chlorite.

Table 1
Modal Analysis *

	Equigranular Rim					
	East	West			South	
	RS MR 5	RS MR 8	RS MR3 6	RS MR3 5	RS SM 1	RS SM 10
quartz	19.6	15.2	22.6	24.4	26.2	15.8
plagioclase	48	65.6	49	43.2	45.4	53.2
orthoclase	24.2	9.8	21.4	21	17.8	22.0
biotite	5.4	6.2	6.0	7.8	8.8	7.0
hornblende	0.2	1	0	0.8	0	0
chlorite	0.2	0.2	0	0.2	0	0.2
titanite	2	0.6	0.2	0.6	0.4	0
apatite	tr	60.2	tr	0.4	tr	0.2
magnetite	0.2	1	0.8	1.6	1.4	0.4
zircon	0.2	0.2	tr	0	tr	tr

Table 1 -- Continued
Modal Analysis

	Porphyry Core		Aplite Dike		Biotite Diorite
quartz	RS MR3 8	RS M	RS MR 4	RS MR 6	D MR2 2
plagioclase	27.8	4.6	18.2	25.2	7.4
orthoclase	45.0	38.4	59.8	39.8	76.8
biotite	20.4	46.8	15	34.4	1.8
hornblende	5.2	9	4.2	tr	6.8
chlorite	0	tr	0	0	**
titanite	tr	0	tr	tr	0.2
apatite	0.06	0	2.2	tr	tr
magnetite	0.2	0.8	0.4	tr	tr
zircon	.4	tr	0.2	0.4	2.4
	tr	0.4	tr	tr	tr

* - modal analyses by David Bero
** - contains 2.2 modal % clinopyroxene

Granodiorite

At the eastern edge of the batholith the border is fine-grained equigranular and grades to a coarse seriate texture near the contact with the porphyritic core. 5 to 20mm potassium feldspar phenocrysts are moderately perthitic at the edge of the batholith, but are microcline in composition near the core. Dark brown biotite occurs predominately as small 1 to 2mm flakes or as aggregates, and rarely as large 5mm, euhedral flakes. Locally minor amounts of small 2 to 5mm, euhedral hornblende occur near the large biotite flakes. These clusters are associated with concentrations of titanite, apatite, zircon, and magnetite. The groundmass consists of anhedral grains of quartz, potassium feldspar, and plagioclase.

Samples along the western edge of the batholith are coarsely equigranular to seriate mosaics of interlocking grains. Potassium feldspar occurs as large 5 to 15mm, subhedral grains and smaller 1 to 5mm, anhedral grains. Both size fractions are mildly to moderately perthitic. Dark to olive brown biotite occurs as large euhedral flakes that contain up to 2 areal percent enclosed grains of apatite, titanite, zircon, and trace amounts of magnetite. Rare small hornblende fragments are partially replaced by fine-grained aggregates of biotite. Trace concentrations of fine-grained anhedral opaque minerals and rutile are intergrown with the biotite clusters.

The southern rim phase is locally porphyritic and is very similar in texture and modal mineralogy to the porphyry core phase. Large, pink, perthitic, euhedral to subhedral orthoclase phenocrysts are scattered in a coarse groundmass of large, rounded quartz "eyes", and lesser amounts of plagioclase laths. Fine-grained aggregates of biotite are common and partially replace rare, relic hornblende fragments. Larger biotite fragments are rare and locally are rimmed by finer grained biotite. Titanite is rare and occurs as fine-grained, embayed fragments partially replaced by a finer grained opaque mineral. The groundmass consists of anhedral grains of orthoclase, quartz, and minor amounts of plagioclase.

The porphyritic core phase is characterized by up to 3cm, pink orthoclase phenocrysts set in a coarse groundmass of interlocking plagioclase laths, round quartz grains, and trace amounts of euhedral biotite. The potassium feldspar phenocrysts are subhedral, mildly perthitic, and exhibit Carlsbad twinning. Dark brown to green biotite occurs predominately as anhedral flakes and rarely as large, euhedral flakes. The rims of the larger flakes are ragged and replaced by finer grained biotite. Biotite and the accessory phases are not uniformly distributed throughout the groundmass, but form clusters interstitial to the porphyritic phases. The groundmass consists of subhedral microcline and perthitic orthoclase, anhedral quartz, and

untwinned plagioclase. No hornblende was observed in any of the porphyritic samples.

Quartz Monzonite

The Ruby Star quartz monzonite is considered to be closely related to the porphyritic core phase and not to represent a distinct intrusive phase as it is interpreted to be by West and Aiken (1982). The modal mineralogy and texture are practically identical except that the quartz monzonite lacks abundant titanite.

CHAPTER 3

PETROLOGY

Whole Rock Chemistry

The whole rock chemical data presented in Table 2 are a combination of data from Skyline analytical lab and neutron activation data gathered by Anthony (Anthony, 1986).

On the basis of the whole rock data, petrographic analysis, and normative compositions presented in this paper, and the trace element work of Anthony (1986) several samples were eliminated as too weathered or as more representative of products of hydrothermal alteration than the primary, magmatic processes of interest in this study. The remaining samples in Table 2 are assumed to represent fresh samples.

SiO_2 values range from a low of about 60 weight percent in the biotite diorite to a high value of 77 weight percent in the late-stage aplite dike. If the samples of the biotite quartz diorite and the aplite dike are neglected, the remaining samples have a total variation in SiO_2 content of 6 weight percent. Because the variation in SiO_2 is small interpretations drawn from the absolute

Table 2
Whole Rock Analysis

	Equigranular Rim					
	East	West			South	
Oxide Wt %	RS MR 5	RS MR 8	RS MR3 6	RS MR3 5	RS SM 1	RS SM 10
SiO2	67.66	68.80	69.97	68.57	68.12	70.25
TiO2	0.43	0.42	0.40	0.42	0.47	0.33
Al2O3	16.07	15.96	15.33	16.33	16.04	15.84
MgO	1.24	0.90	0.90	0.90	1.45	0.78
Fe2O3	3.47	3.18	3.22	2.93	3.92	2.21
CaO	3.25	2.84	2.64	2.72	3.07	2.16
Na2O	4.01	4.27	3.96	4.20	3.99	4.03
K2O	3.82	3.59	3.55	3.89	2.90	4.38
MnO	0.05	0.04	0.03	0.04	0.04	0.02
Total *	100.00	100.00	100.00	100.00	100.00	100.00
TOTAL	97.10	98.39	98.48	98.00	96.61	100.36

* normalized to 100

CIPW Normative Analysis

	RS MR 5	RS MR 8	RS MR3 6	RS MR3 5	RS SM 1	RS SM 10
quartz	19.65	21.28	22.27	20.8	22.94	22.74
corundum	0	0	0	0.12	0.54	0.02
orthoclase	21.92	20.85	23.16	22.51	16.54	26
albite	32.91	36.38	34.69	35.02	33.16	35.36
anorthite	14.14	13.11	12.85	13.48	14.93	11.55
diopside	1.45	0.53	0.49	0	0	0
hedenbergite	0.68	0.3	0.28	0	0	0
enstatite	2.31	1.96	2.01	2.19	3.48	1.94
ferrosilite	1.25	1.3	0.32	1.29	1.74	0.96
magnetite	1.95	1.81	1.84	1.66	2.2	1.29
ilmenite	0.79	0.77	0.77	0.77	0.85	0.62
hematite	0	0	0	0.7	0	0

Table 2 -- Continued
Whole Rock Analysis

Oxide Wt %	Porphyry Core RS MR3 8	RS MR3 2	:	Aplite Dike RS MR 4	RS MR 6	:	Biotite Quartz Diorite D MR2 2	D MR2 3
SiO2	70.93	69.33	:	71.29	77.44	:	60.96	61.63
TiO2	0.28	0.37	:	0.29	0.10	:	0.70	0.67
Al2O3	15.65	16.24	:	15.10	12.52	:	17.27	17.21
MgO	0.66	0.82	:	0.56	0.05	:	2.16	2.02
Fe2O3	2.31	2.96	:	1.92	0.67	:	6.32	5.93
CaO	2.08	2.38	:	1.66	0.70	:	5.04	4.93
Na2O	4.04	4.10	:	3.74	2.95	:	3.98	3.90
K2O	4.01	3.78	:	5.42	5.56	:	3.48	3.62
MnO	0.04	0.02	:	0.02	0.01	:	0.09	0.09
Total *	100.00	100.00		100.00	100.00		100.00	100.00
TOTAL	98.42	98.51		97.35	99.05		97.28	98.81

* normalized to 100

CIPW Normative Analysis

	RS MR3 8	RS MR3 2	:	RS MR 4	RS MR 6	:	D MR2 2	D MR2 3
quartz	24.93	23.78	:	23.23	36.78	:	10.55	10.51
corundum	0.49	0.94	:	0	0.3	:	0	0
orthoclase	23.34	Q21.98	:	31.2	32.55	:	20.03	21.15
albite	34.35	33.67	:	31.13	24.87	:	31.3	33.84
anorthite	10.78	12.23	:	7.99	3.53	:	19.21	17.85
diopside	0	0	:	0.29	0	:	3.44	3.40
hedenbergite	0	0	:	0.15	0.03	:	1.78	1.75
enstatite	1.61	2.01	:	1.2	6	:	3.63	3.40
ferrosilite	1.1	1.37	:	0.72	0.27	:	2.15	2.00
magnetite	1.31	1.69	:	1.08	0.39	:	3.56	3.40
ilmenite	0.53	0.68	:	0.53	0.18	:	1.29	1.25
hematite	0	0	:	0	0	:	0	0

variation in increasing or decreasing oxide concentrations with SiO_2 content should be guarded.

All the samples show a consistent decrease in the major elements, except Na_2O and K_2O, with increasing SiO_2 content of the sample (see Figure 3). All the figures show a large separation of sample compositions between the biotite quartz diorite and the two members of the Granodiorite and an overlap of sample compositions between the equigranular and the porphyritic members of the Granodiorite.

Plots of weight percent oxide whole-rock data on CaO-Na_2O-K_2O and AFM ternaries have a trend similar to the trend of progressive calc-alkaline differentiation (see Figures 4.1 and 4.2).

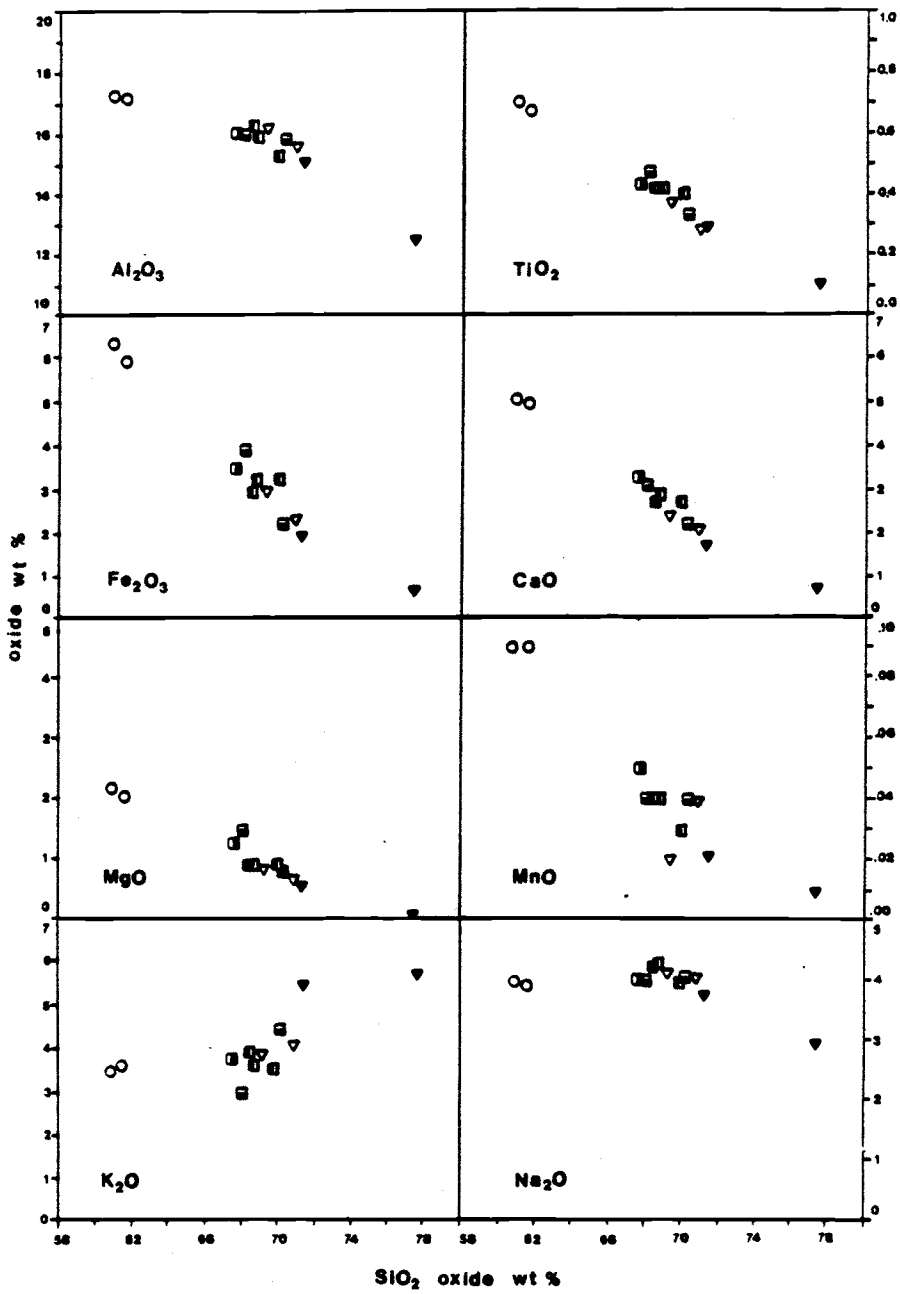

Figure 3. Whole Rock Variation Diagram

Plot of the major oxides in weight percent against SiO_2 weight percent oxide for each sample. Total iron is calculated as Fe_2O_3. Symbols as in Figure 2.

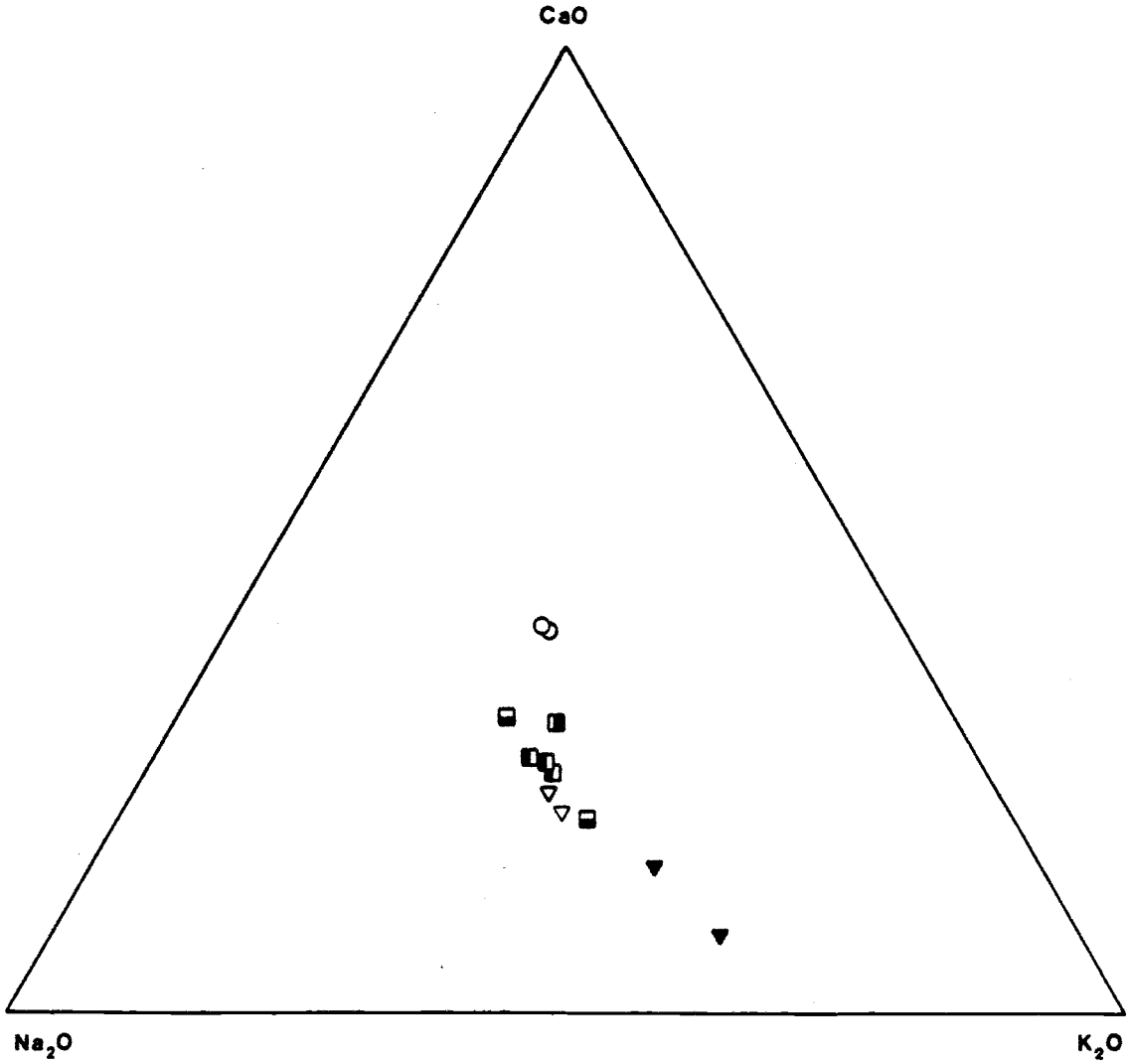

Figure 4.1. $CaO-Na_2O-K_2O$ Ternary.

Plot of whole-rock oxide weight percent data on $CaO-Na_2O-K_2O$ ternary.

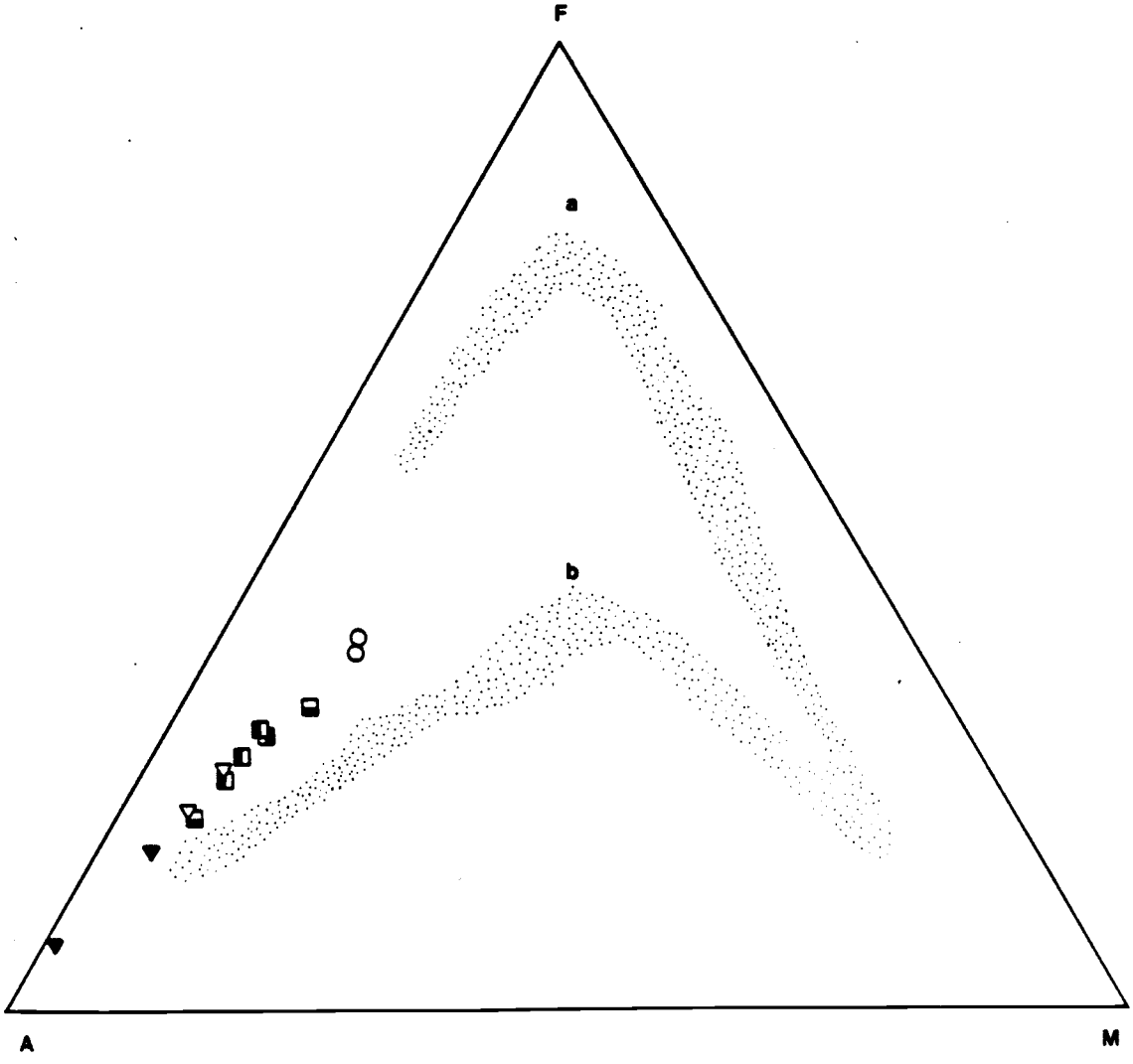

○ biotite quartz diorite
granodiorite equigranular rim
◨ east rim
◧ west rim
◒ south rim
▽ granodiorite porphyritic core
▼ aplite dike

Figure 4.2. AFM Ternary.

Plot of whole-rock oxide weight percent data on an AFM ternary, where A = Na_2O + K_2O, F = total iron calculated as Fe_2O_3, and M = MgO. Path (a) is an iron enrichment trend typical of tholeiitic suites. Path (b) is typical of the calc-alkaline trend. After Barker (1983).

CHAPTER 4

CRYSTAL CHEMISTRY

The crystal chemistry of biotite, hornblende, the plagioclase and alkali feldspars, magnetite, and apatite are discussed below.

Analytical Technique

Petrograghic examination and electron microprobe analysis were performed on standard petrographic thin sections with a high polish. Electron microprobe analyses were performed on a four channel SEMQ at an 15kV accelerating potential. A 15 nanoampere sample current was used for analysis of major elements. The beam diameter was 30 microns and each element was analyzed for 40 to 90 seconds. All microprobe runs were proceeded and followed by a series of analyses performed on standard unknowns provided by the Smithsonian Institution. The standard for most elements were Kakanui hornblende, Kakanui augite and Juan de Fuca Ridge glass. The fluorine standard was fluro-apatite and the chlorine standard was scapolite. All element calibrations were within 2 percent deviation of the standard unknowns. Weight percent oxide concentrations were reduced

from raw k-ratio data by computerized Bence-Albee data files.

Biotite

Biotites chosen for microprobe analysis were 2 to 5mm, euhedral grains with no apparent chloritization. Only those biotites that were oriented with the c-axis parallel to the electron beam were analyzed to insure the uniformity among the biotite analyses. Ca and the alkali-site concentrations of Na and K seemed most sensitive to the relative orientation of the biotite to the electron beam. No indication of zoning was found in any of the biotites.

The ferric to ferrous iron content of five biotite samples as well as the lattice site occupancy was determined by M. Darby Dyar of MIT by Mossbauer analysis. Two additional biotite samples, mineral separates purified by hand under a binocular microscope, were analyzed for total iron and ferrous iron by Kurt Fredriksson at the Smithsonian Institution.

Hornblende

The hornblendes chosen from microprobe analysis were 2 to 4mm euhedral grains. In the southern equigranular rim phase, where only fragments of relic grains remained, only the centers of larger grains were analyzed. At least three hornblendes were analyzed from each sample and each grain was analyzed at least three times. Initial analyses

on a tight grid pattern failed to show any zoning or systematic chemical variation across the hornblende grains.

Feldspars

Two groups of feldspars were analyzed from most of the samples. One group was analyzed for barium, strontium, and iron in addition to the major oxide components of feldspar. The first group of analyses was used to determine the variation in minor element chemistry among members of the magmatic suite. The second group consisted of small, anhedral groundmass feldspars and was analyzed only for the major oxide components. The second group of feldspar analyses was used to estimate the eutectic temperature for each member by two-feldspar thermometry. Petrographic analysis indicated that many of the potassium feldspars from the equigranular and porphyritic granodiorite are microscopically perthitic. A total potassium feldspar analysis consisting of the perthite and the host alkali feldspar was obtained by using a wide electron beam. Other workers have attempted to integrate the total potassium feldspar composition by setting up a grid work of focused beam analyses, and integrating data points to obtain the solvus composition (Czamanske and others, 1981). I believe there is less error in the first method if an appropriate beam width and sample current are used.

Magnetite

Electron microprobe analyses of iron oxides in all samples indicated the iron oxide is magnetite. No ilmenite or other Ti-Fe oxide was identified in any sample. Pyrite occurs in trace concentrations in two samples from the southern equigranular rim.

Apatite

The fluorine and chlorine content of apatite from six samples were analyzed by electron microprobe. All analyzed apatites are enclosed grains in biotite. The small size of the apatites required a more tightly focused electron beam (15 to 20 microns).

Crystal Chemistry

Biotite

Representative biotite analyses and stoichiometry are presented in Table 3. The Fe/(Fe + Mg) content in biotite is plotted against the total Al content in Figure 5. The biotites plot closest to the phlogopite end member. The variation in the major element composition of the biotite versus the Fe/(Fe + Mg) ratio is shown in Figure 6. All of the biotites from the Granodiorite are very similar in composition. The variation in the Fe/(Fe + Mg) ratio is small. A nearly constant Fe/(Fe + Mg) ratio has been interpreted to reflect hydrothermal alteration or subsolidus

Table 3
Representative Biotite Analysis

	Equigranular Rim East	Equigranular Rim West			South	Porphyry Core		Biotite Diorite
	RS MR 5	RS MR 8	RS MR3 6	RS MR3 5	RS SM 1	RS MR3 8	RS MR3 2	DMR2 3
SiO2	37.68	37.57	37.14	36.82	37.23	37.98	36.34	37.90
Al2O3	13.32	14.31	15.27	14.13	14.73	13.80	15.03	13.91
Tio2	3.90	3.13	3.05	3.08	3.70	3.12	3.36	2.46
Feo(T)	17.35	16.80	17.36	16.56	16.97	16.07	18.12	18.56
Mgo	13.32	13.98	13.19	13.72	12.85	13.89	12.06	12.89
Cao	0.01	0.00	0.01	0.03	0.00	0.00	0.05	0.06
Mno	0.51	0.55	0.36	0.55	0.32	0.66	0.22	0.30
Na2O	0.06	0.08	0.07	0.06	0.10	0.10	0.12	0.07
K2O	9.46	9.19	9.46	9.20	9.52	9.41	8.99	8.53
F	0.30	0.43	0.60	0.30	0.63	0.96		0.46
CL	0.02	0.02	0.04	0.49	0.05	0.03		0.06
TOTAL	95.93	96.06	96.55	94.94	96.10	96.02	94.29	95.20
Si	5.6712	5.6167	5.5420	5.5914	5.5758	5.6696	5.5701	5.7331
Al	2.1759	2.3833	2.3713	2.2613	2.2542	2.1900	2.2673	2.2669
Fe3+	0.1529	0.0000	0.0867	0.1472	0.1700	0.1404	0.1626	0.0000
Al	0.1876	0.1388	0.3150	0.2684	0.3466	0.2387	0.4486	0.2137
Fe3+	0.3276	0.6305	0.3250	0.3155	0.1275	0.2809	0.3484	0.1850
Ti	0.4415	0.3519	0.3423	0.3518	0.4167	0.3503	0.3873	0.2799
Mg	2.9878	3.1148	2.9333	3.1051	2.8681	3.0902	2.7549	2.9059
Fe2+	1.7035	1.4712	1.7548	1.6405	1.8280	1.5849	1.8118	2.1630
Mn	0.0650	0.0696	0.0695	0.0707	0.0406	0.0835	0.0286	0.0384
Ca	0.0016	0.0000	0.0016	0.0049	0.0000	0.0000	0.0082	0.0097
Na	0.0175	0.0232	0.0174	0.0177	0.0290	0.0289	0.0357	0.0205
K	1.8165	1.7528	1.7514	1.7824	1.8190	1.7921	1.7580	1.6462
A site	1.8356	1.7760	1.7704	1.8050	1.8480	1.8211	1.8019	1.6764
VI site	5.7130	5.7769	5.7399	5.7519	5.6275	5.6283	5.7796	5.7859
Fe/Fe+Mg	0.4223	0.4029	0.4248	0.4038	0.4256	0.3937	0.4575	0.4469

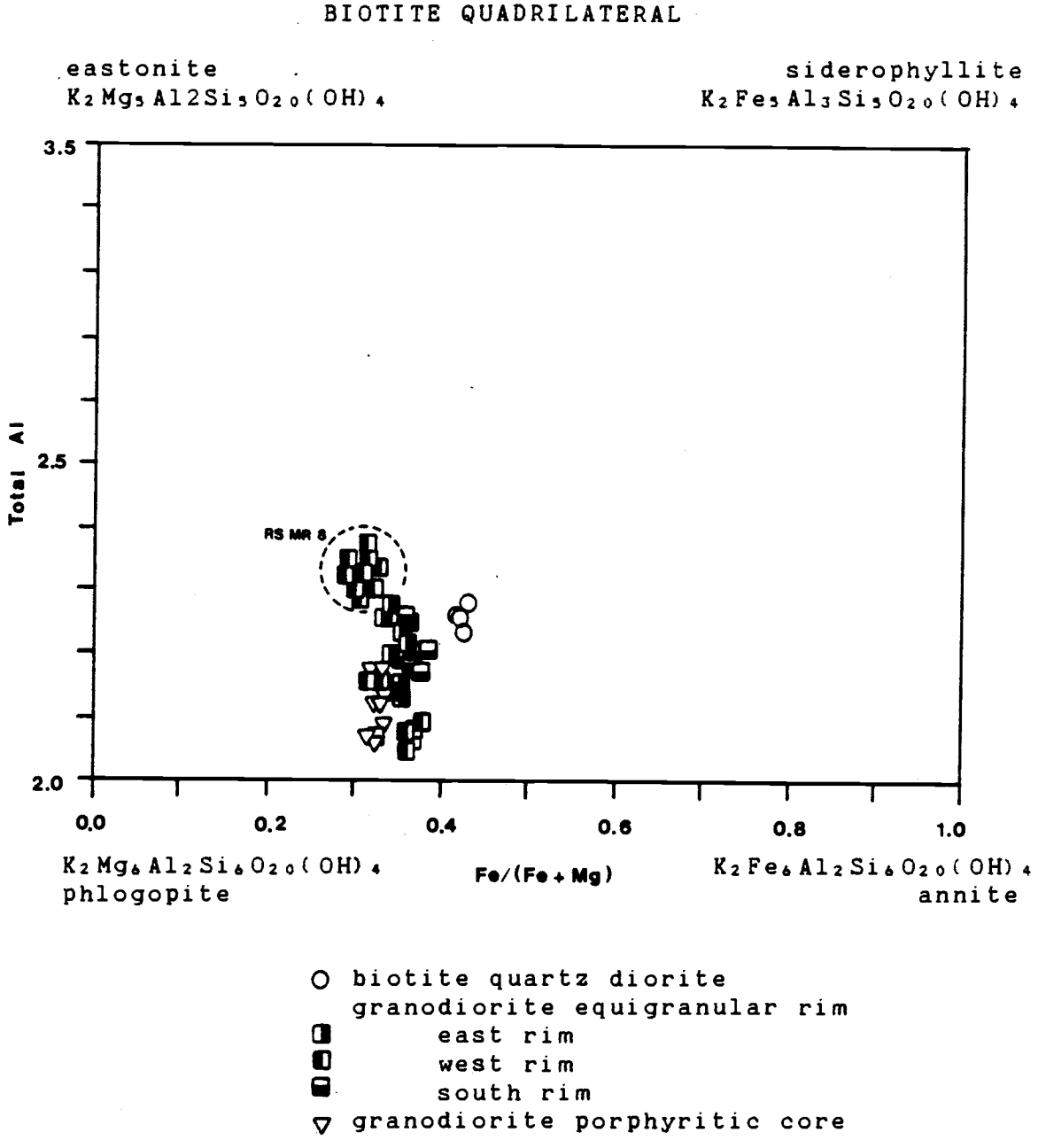

Figure 5. Biotite Quadrilateral.

A plot of the ratio Fe^{2+}:Mg vs Al in biotite superimposed on the biotite quadrilateral of Speer (1984). The range in the Fe^{2+}:Mg ratio is limited but clearly decreases from the biotite-quartz diorite to the granodiorite. The range in Al values is larger and also decreases in concentration from the biotite-quartz diorite to the granodiorite.

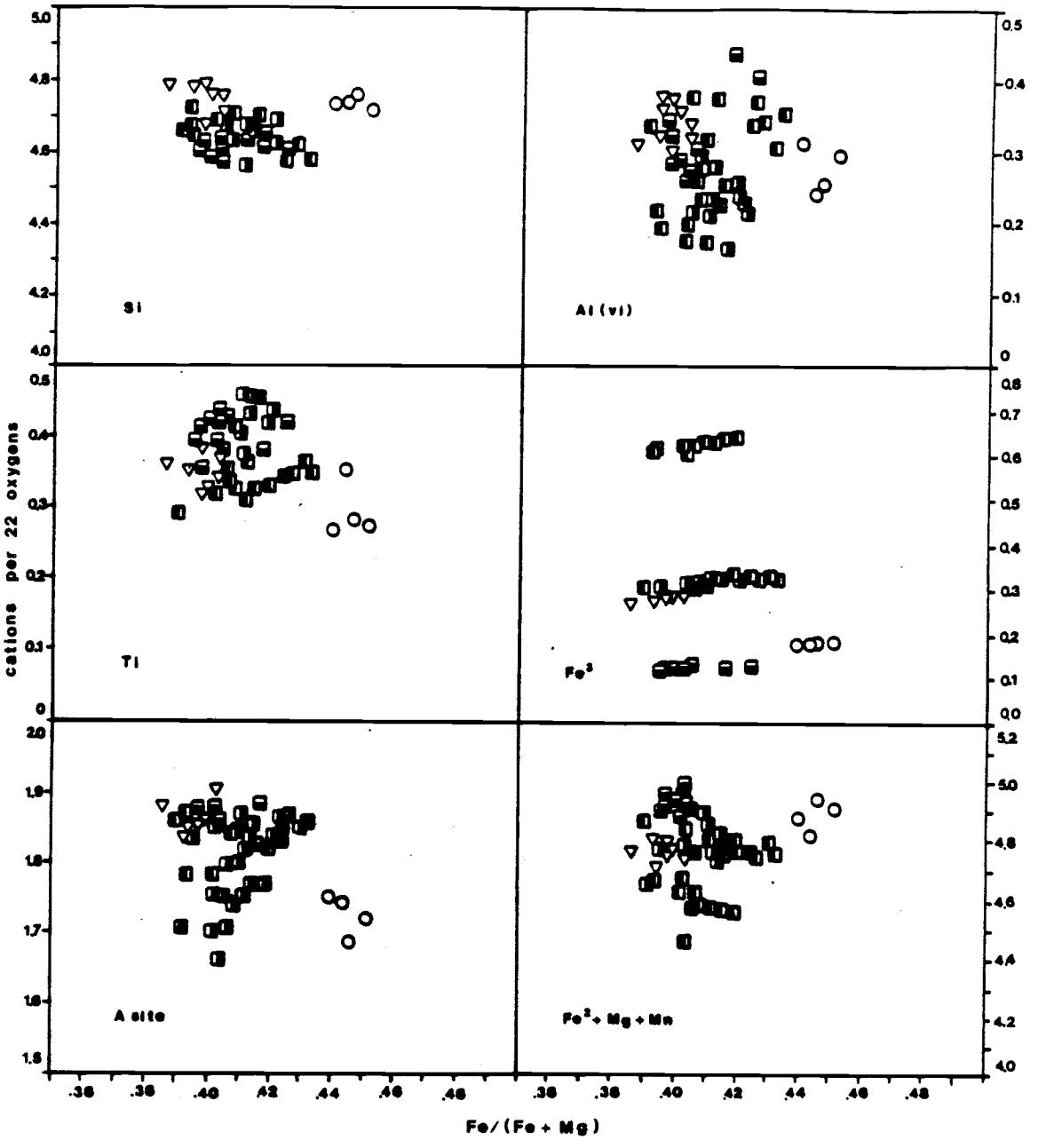

Figure 6. Biotite Crystal Chemistry vs Fe/(Fe + Mg) Ratio in Biotite

The major cations constituents of biotite are plotted against their Fe/(Fe + Mg) content. The biotites from the Granodiorite are all similar in composition and show no systematic variation in major cations with the Fe/(Fe + Mg) content. Fe^{3+} refers to Fe^{3+} content of the octahedral layer as determined by Mossbauer spectroscopy. Symbols as in Figure 5.

re-equilibration (Dodge and Moore, 1968; Speer, 1984). In this study the Fe/(Fe + Mg) ratio shows no systematic variation with spacial proximity to porphyry copper mineralization or with any other parameter related to hydrothermal alteration; therefore, I do not believe that the limited variation in the Fe/(Fe + Mg) ratio is a result of alteration. However, the Fe/(Fe + Mg) ratio could reflect subsolidus re-equilibration.

When the Fe/(Fe + Mg) ratio in biotite and the same ratio in the host rock are plotted against the SiO_2 content of the host rock, the biotite composition and host rock composition show diverging trends (see Figure 7). The host rock continues to become more Fe-rich while the biotites become progressively more Mg-rich as Mg is preferentially partitioned into the biotite. The paired Fe-depletion in biotite and Fe-enrichment in the host rock suggests that less Fe^{2+} was available to enter biotite and Fe^{3+} was precipitated as magnetite as the host rock crystallized (Mueller, 1972; Mueller, 1969; Osborn, 1962).

In Figure 8 the Fe^{2+}- Fe^{3+}- Mg content of biotites are plotted on a ternary with various ferrous-ferric iron buffers. The Fe^{3+} and Mg content of the biotites increases from the biotite diorite to the porphyritic granodiorite.

The fluorine and chlorine content of the hydroxyl site can be used as a means of determining the origin of the biotites (Munoz, 1984). However, the fluorine and chlorine

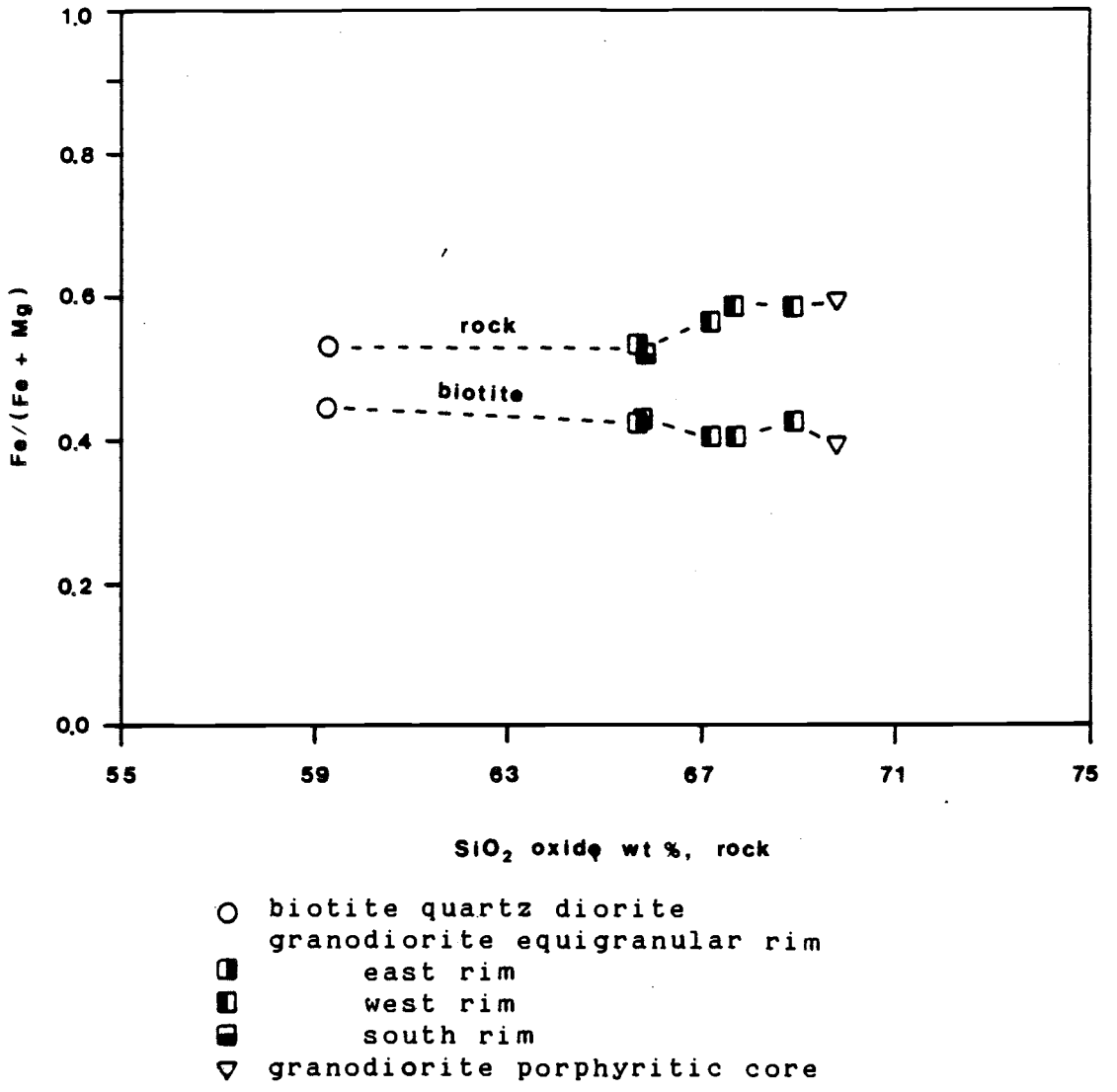

Figure 7. Fe/(Fe + Mg) Ratios in Biotite and Host Rock vs. SiO_2 Content of the Host Rock.

A plot of the Fe/(Fe + Mg) content of biotite and the host rock against the SiO_2 oxide weight percent in the host rock. The diverging trends in the Fe:Mg ratio of the biotite and the same ratio in the host rock indicate crystallization under progressively more oxidizing environments (Bailey, 1984; after Murakami, 1969).

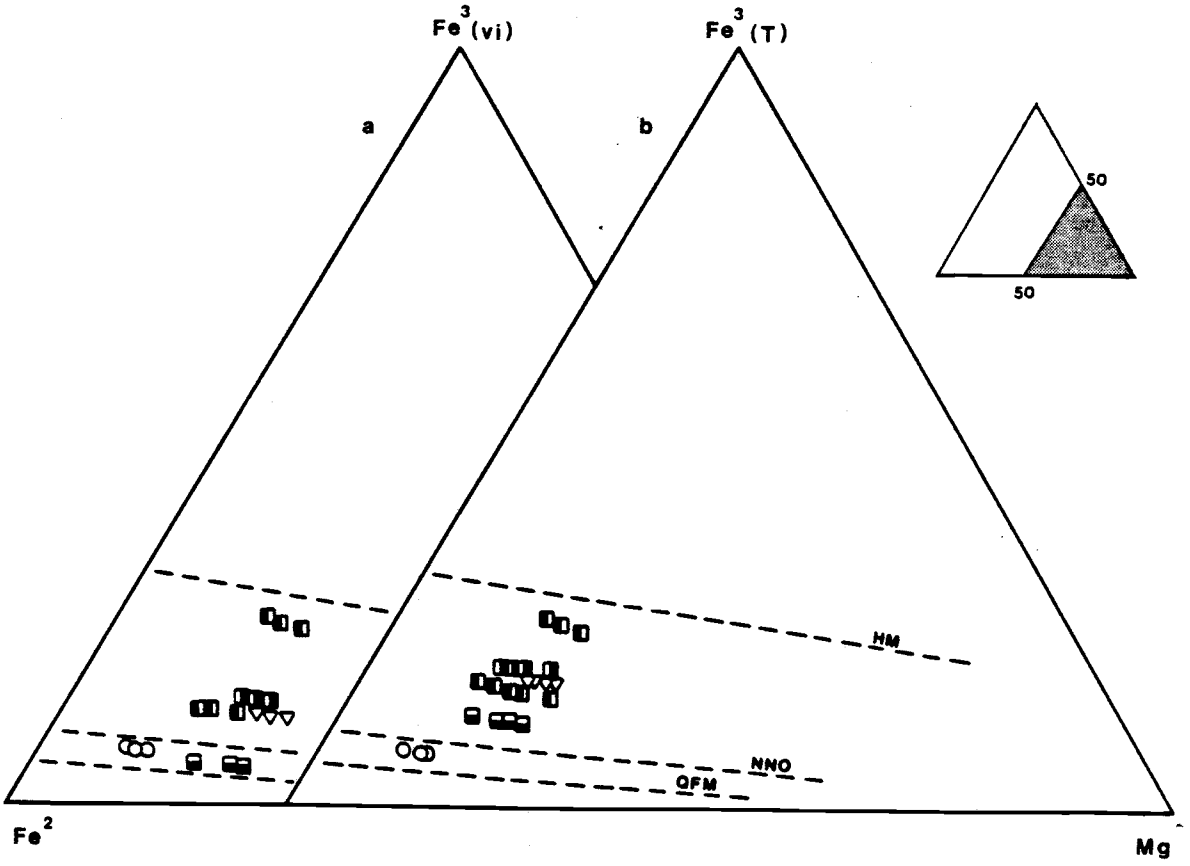

○ biotite quartz diorite
granodiorite equigranular rim
▮ east rim
◧ west rim
▬ south rim
▽ granodiorite porphyritic core

Figure 8. Fe^{2+}-Fe^{3+}-Mg Ternary.

The Fe^{2+}-Fe^{3+}-Mg plot of the octahedral site occupancy of the Ruby Star biotites plotted on a ternary representing the biotite end member compositions. In (a) the amount of Fe^{3+} in the octahedral site was determined by Mossbauer spectroscopy. In (b) all Fe^{3+} is assigned to the octahedral site to allow comparison of the Ruby Star biotites to biotites of other studies where the distribution of Fe^{3+} between the octahedral and tetrahedral site was not determined.

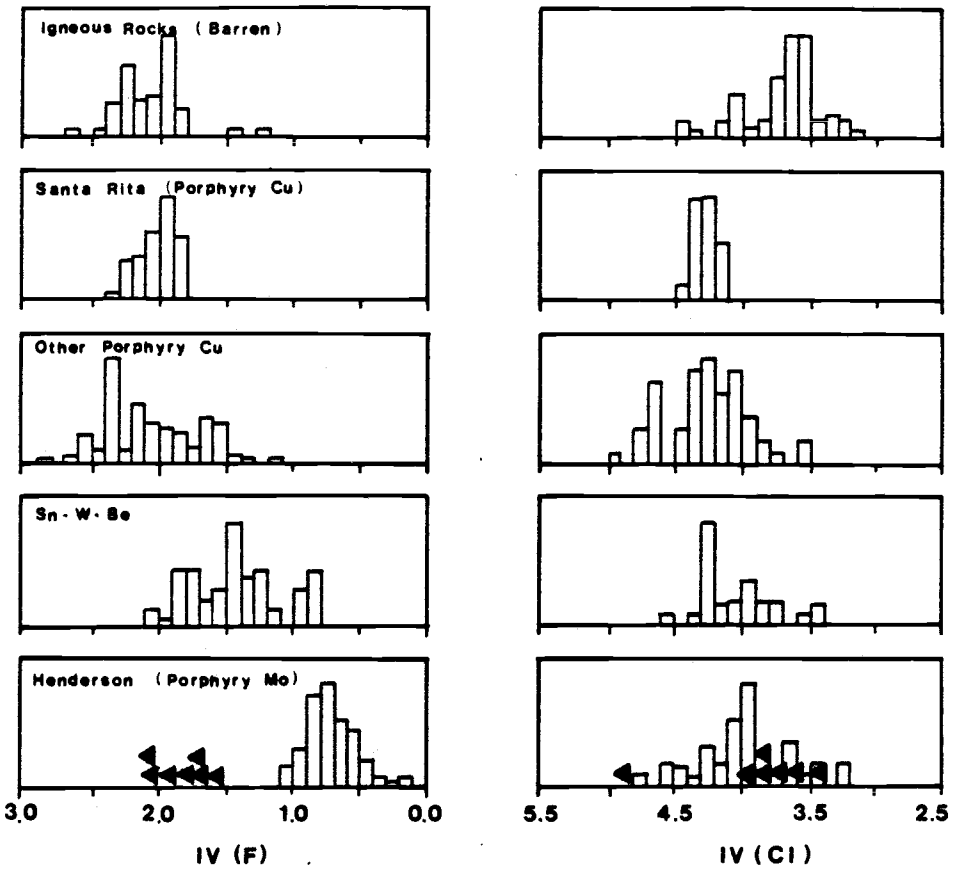

Figure 9. Biotite Fluorine and Chlorine Intercept Values.

Histograms of F and Cl intercept values of biotites from various environments. Relative increase in fluorine is to the right; relative increase in chlorine is to the left (Munoz, 1984). The shaded triangles at the bottom are biotites from this study. The height of the solid triangles have no relationship to the height of the columns and show only the distribution of the F and Cl intercept values.

content of the hydroxyl site is influenced by the composition of the octahedral layer through the mechanisms of Fe-F avoidance and Mg-Cl avoidance. Munoz (1984) devised a method to compare the fluorine and chlorine content of biotites independently of their iron and magnesium content by defining fluorine and chlorine intercept values:

(4.1) $IV(F)_{bio} = 1.52\ X_{Mg} + 0.42\ X_{An} + 0.20\ X_{Sid} - \log\ (X_F / X_{OH})$

(4.2) $IV(Cl)_{bio} = -5.01 - 1.93\ X_{Mg} - \log\ (X_{Cl} / X_{OH})$

where X_{Mg}, X_{An}, and X_{Sid} are the mole fractions of phlogopite, annite, and siderophyllite in biotite. Figure 9 is a histogram showing representative fluorine and chlorine intercept values of biotites from many different environments. The biotites from this study have intercept values most similar to biotites from igneous environments.

Hornblende

Representative hornblende analyses are listed in Table 4. The Fe/(Fe + Mg) content of the hornblende is plotted against the total Al content in Figure 10. The hornblendes have a compositional range from magnesio-actinolite to magnesio-hornblende.

Many authors have attempted to use the variation in the crystal chemistry of hornblende and co-existing biotite as an indicator of dehydration and redox conditions in granitoid complexes. In general these attempts have been

Table 4
Representative Hornblende Analyses

	Equigranular Rim				
	East	West			South
	RS MR 5	RS MR 8	RS MR3 6	RS MR3 5	RS SM 1
SiO2	51.82	50.47	53.42	50.76	51.21
Al2O3	4.01	4.13	2.51	4.25	4.22
Tio2	0.63	0.51	0.23	0.7	0.59
FeO (T)	11.63	12.72	11.75	12.71	11.25
Mgo	17.01	15.48	16.67	15.27	15.97
Cao	11.71	12	12.01	11.59	11.67
Mno	0.66	0.81	0.55	1.03	0.62
Na2O	0.68	0.68	0.44	0.8	0.57
K2O	0.33	0.32	0.17	0.39	0.33
TOTAL	98.48	97.12	97.75	97.49	96.43
Si	7.4152	7.3877	7.6717	7.3992	7.4654
Al(IV)	0.5848	0.6123	0.3283	0.6008	0.5346
Al(VI)	0.0921	0.1005	0.0964	0.1295	0.1907
Ti	0.0692	0.2246	0.0244	0.0763	0.0647
Mg	3.6271	3.3770	3.5687	3.3180	3.4696
Fe	1.2116	1.0734	1.2861	1.3999	1.2103
Fe	0.1803	0.4838	0.1251	0.1498	0.1613
Mn	0.0796	0.1004	0.0662	0.1269	0.0766
Ca	1.7954	1.8821	1.8475	1.8095	1.8229
K	0.0602	0.0598	0.0320	0.0720	0.0614
Na	0.1899	0.1930	0.1214	0.2256	0.1611
A site	0.2501	0.2528	0.1534	0.2976	0.2225
M4	2.0553	2.4664	2.0388	2.0862	2.0607
Fe/Fe+Mg	0.2773	0.3156	0.2834	0.3184	0.2833

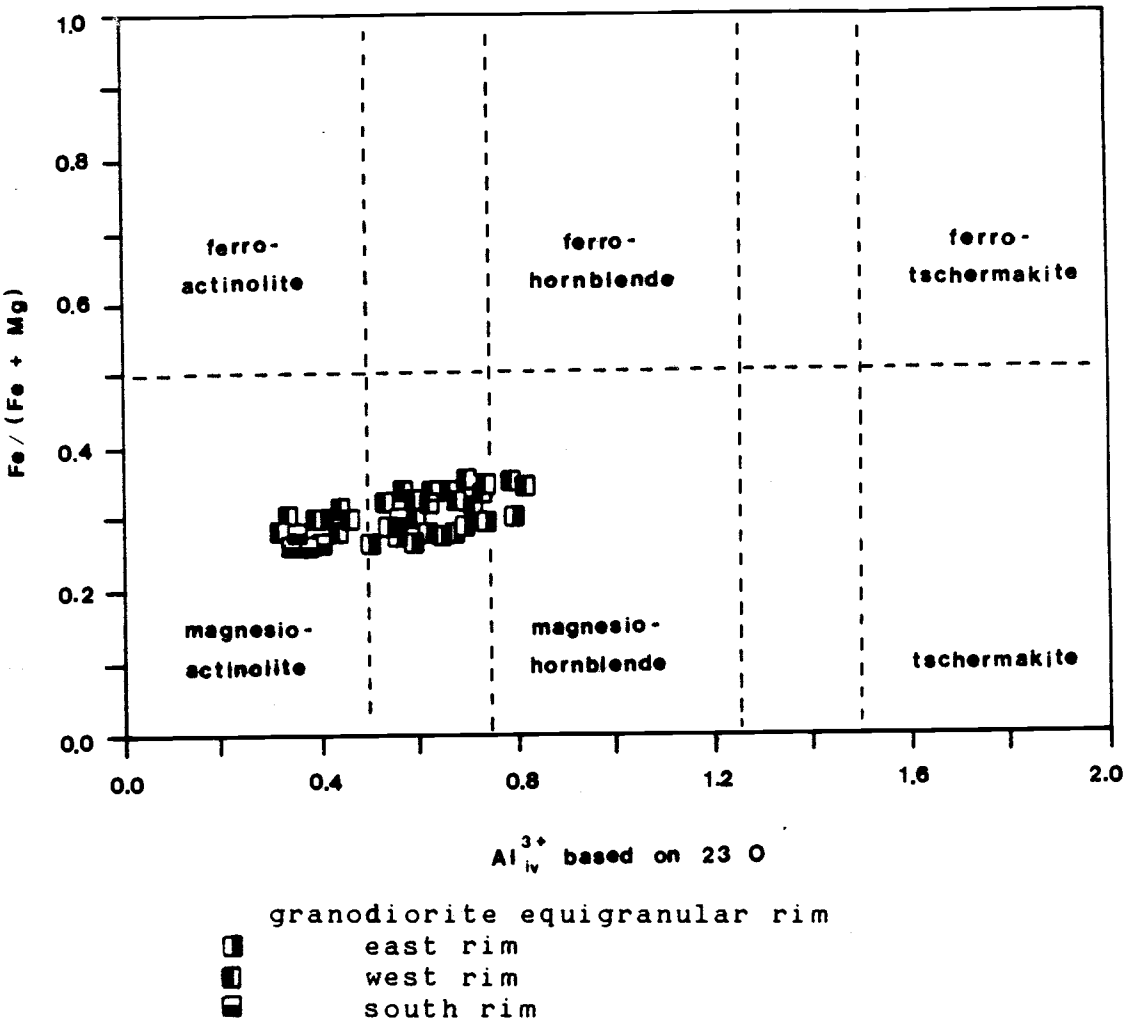

Figure 10. Hornblende Quadrilateral.

All the hornblendes exhibit relatively constant Fe/(Fe + Mg) proportions. The tetrahedral Al content shows more variation extending from the magnesium actinolite field into the true magnesium hornblende field.

frustrated by the complex structure and chemical nature of biotite and hornblende (Speer, 1984). Recent studies (Hammarstrom and Zen, 1985; Hammarstrom and Zen, 1983; Peters et al., 1985) have focused on the Al content of hornblende.

Hammarstrom and Zen (1983) found that the tetrahedrally coordinated Al content is positively correlated to the total Al content in hornblendes in many granitoid complexes. When hornblendes form complexes of similar bulk composition and modal assemblages were compared they found that hornblendes from complexes at pressures of about 10 kbar had consistently higher total Al and tetrahedral Al contents than those hornblende from complexes that crystallized at lower pressure. In 1985, Hammarstrom and Zen provided a quantitative estimate of pressure based on the total Al content:

(4.3) $P(kbar) = -3.89 + 5.04\ Al^{T}$.

Figure 11.1 is a plot of the Ruby Star hornblendes. They show the predicted positive correlation between total Al and tetrahedrally coordinated Al. However, when Equation 4.3 is applied to the Ruby Star hornblendes it produces low and negative pressures. In addition, the results from Equation 4.3 indicate that the total pressure decreased 2200 bars during the crystallization of the Granodiorite, whereas previous work (Mauger, 1966) suggested that the Granodiorite crystallized under essentially isobaric conditions. The

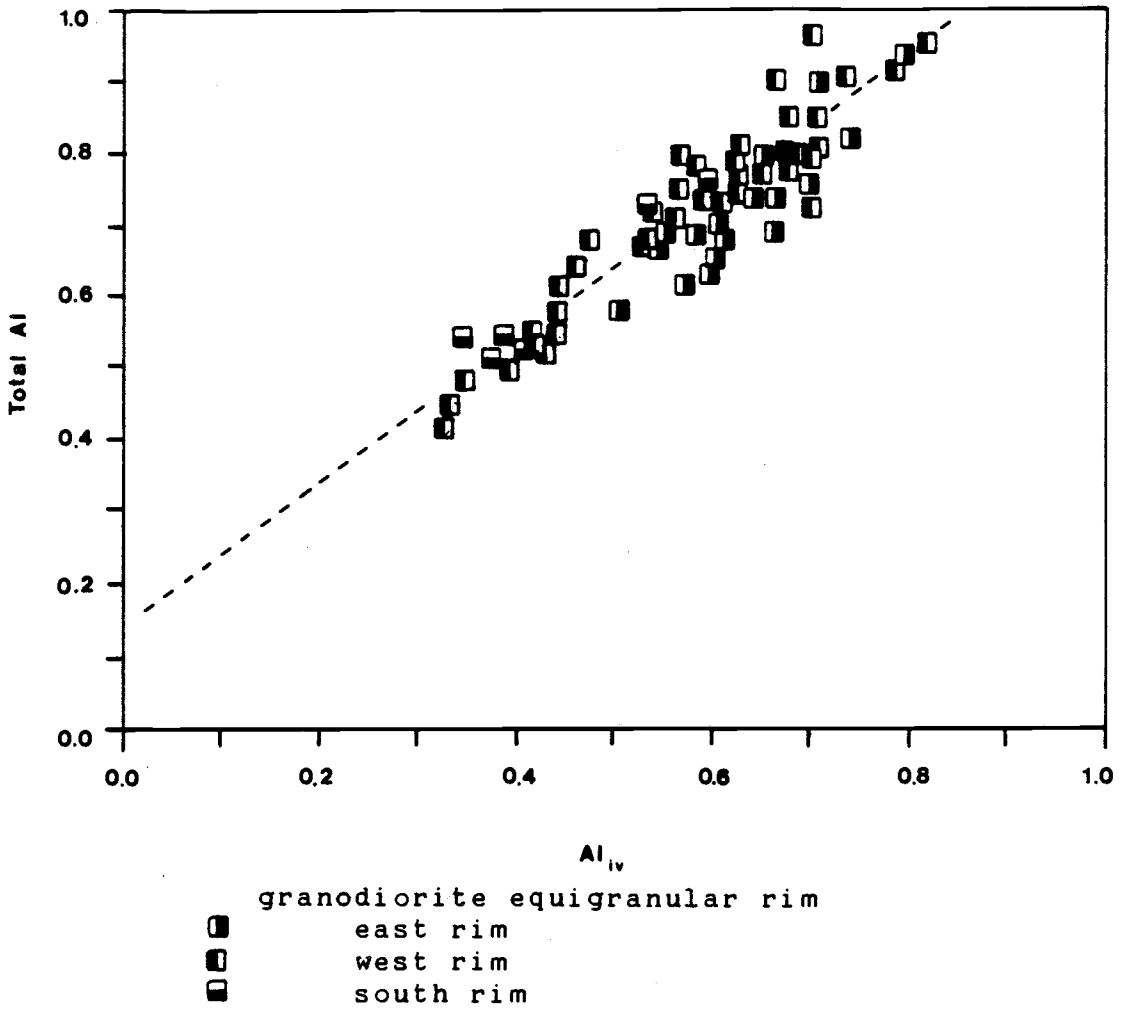

Figure 11.1. **Tetrahedral Al vs. Total Al**

A plot of tetrahedrally coordinated Al vs. total Al has a slope of 1:1. The south and eastern rim have the lowest total Al and tetrahedral Al contents suggesting crystallization at lower pressures.

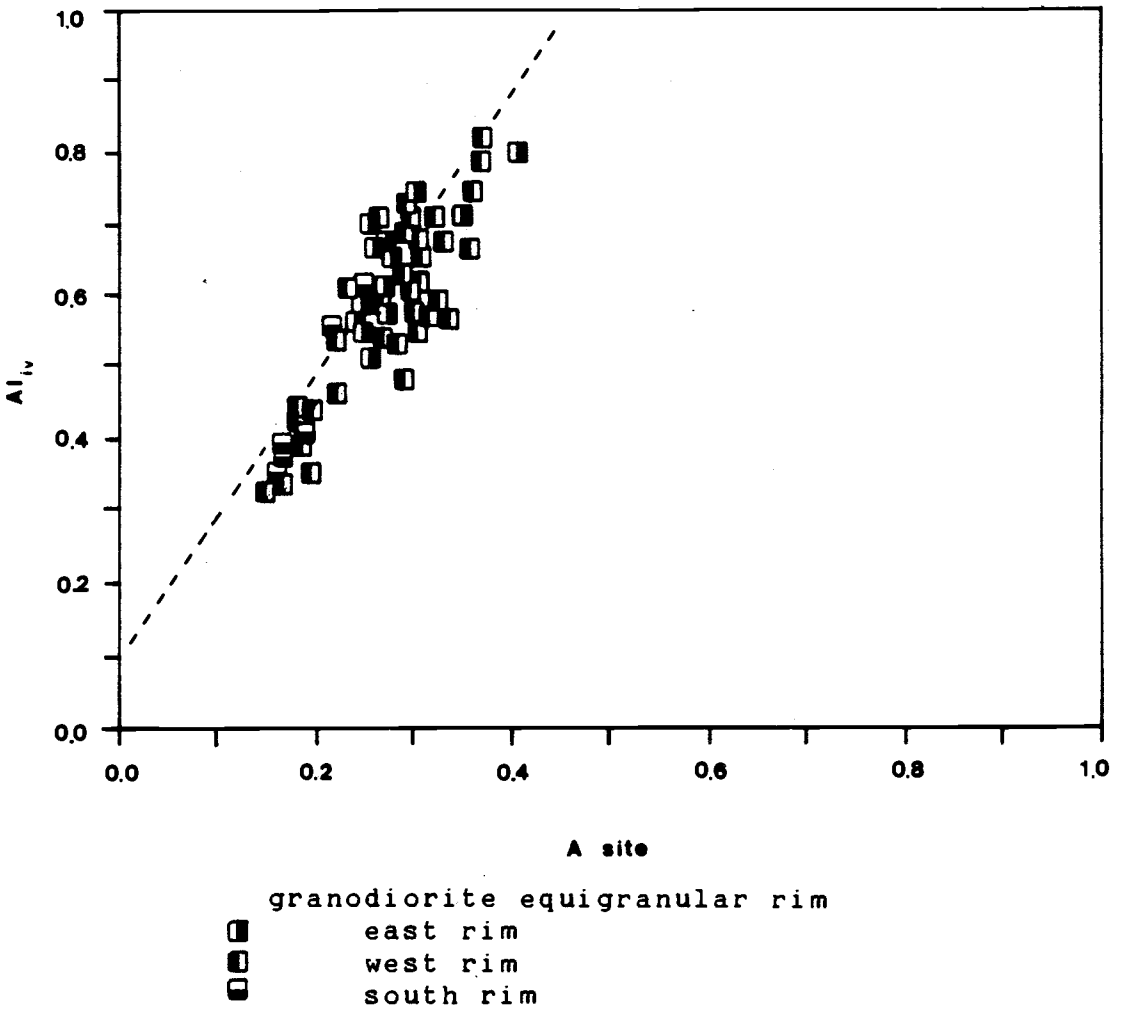

Figure 11.2. **A-site vs. Tetrahedral Al.**

A plot of the total A-site cations, Na + K, against tetrahedrally coordinated Al has a slope of 1:2. The south and eastern rim have the lowest A-site and tetrahedral Al contents suggesting crystallization at lower temperatures.

failure of Equation 4.3 to produce reasonable results in this case may indicate that the correlation between total Al and tetrahedrally coordinated Al is relfects bulk composition constraints.

Peters and others (1985) found that the content of the A-site in hornblende is positively correlated to tetrahedrally coordinated Al and suggested that the increase in A-site occupancy may charge balance the Al substituting for Si in the tetrahedral site. Other authors have suggested that the relationship between the A-site content and the tetrahedral Al content may be temperature dependent (Wones and Gilbert, 1982). Low A-site and tetrahedral Al content indicates low temperature. Figure 11.2 is a plot of the A-site occupancy against tetrahedral Al.

Feldspars

Table 5 contains representative feldspar analyses. The major element composition of the potassium feldspar shows little variation. The barium concentration varies from 0.1 to 0.4 oxide weight percent. The higher barium concentrations are found in the biotite diorite and the lower values are found in the porphyritic core phase.

The composition of the plagioclase feldspar varies in composition from andesine in the biotite diorite to albite in the groundmass of the porphyritic core phase. Plagioclase contains iron concentrations between 0.2 and 0.4

Table 5
Representative Feldspar Analyses

	Equigranular Rim East	Equigranular Rim West	Equigranular Rim South	Porphyry Core	Aplite Dike	Biotite Diorite
	RS MR 5	RS MR 8	RS SM 1	RS MR3 8	RS MR 4	DMR2 3
alkali feldspars						
K2O	15.41	14.58	15.43	14.83	15.62	15.24
Na2O	0.99	1.50	0.84	1.40	0.74	0.94
CaO	0	0.02	0	0.06	0	0
Al2O3	18.42	18.63	18.08	18.29	18.65	18.73
SiO2	64.85	65.20	64.53	65.24	64.98	64.98
TOTAL	99.67	99.93	98.88	99.82	99.99	99.89
Si	2.9926	2.9969	3.0068	3.0017	2.9944	2.9928
Al	1.0016	1.0090	0.9930	0.9920	1.0126	1.0163
Ca	0	0.0011	0	0.0029	0	0.0002
Na	0.0887	0.1336	0.0762	0.1247	0.0660	0.0838
K	0.9073	0.8491	0.9171	0.8703	0.9180	0.8953
O site	0.9960	0.9838	0.9933	0.9979	0.9840	0.9793
T site	3.9942	4.0059	3.9998	3.9937	4.0070	4.0091
plagioclase cores						
K2O	0.42	0.23	0.28	0.46	0.17	0.13
Na2O	7.88	6.38	8.13	8.04	8.16	7.34
CaO	6.39	8.06	4.89	5.86	4.85	6.74
Al2O3	24.67	26.95	23.88	24.32	23.68	25.26
SiO2	60.28	58.08	62.70	61.16	62.94	60.81
TOTAL	99.64	99.70	99.88	99.84	99.80	100.28
Si	2.6922	2.5943	2.7725	2.7209	2.7826	2.6924
Al	1.2922	1.4188	1.2446	1.2709	1.2338	1.3178
Ca	0.3057	0.4001	0.2315	0.2782	0.2295	0.3195
Na	0.6823	0.5525	0.6970	0.6933	0.6992	0.3020
K	0.0239	0.0131	0.0159	0.0259	0.0096	0.0073
O site	1.0119	0.9657	0.9444	0.9974	0.9383	0.6288
T site	3.9844	4.0131	4.0171	3.9918	4.0164	4.0102
plagioclase rims						
K2O	0.32	0.30	0.31	0.29	0.15	0.14
Na2O	7.98	7.80	8.21	8.51	10.62	7.40
CaO	6.32	5.66	4.94	5.09	0.40	6.24
Al2O3	24.84	24.42	23.68	23.73	20.10	24.96
SiO2	60.08	61.41	62.95	62.33	68.77	61.04
TOTAL	99.54	99.59	100.09	99.95	100.04	99.78
Si	2.6844	2.7323	2.7789	2.7593	2.9919	2.7106
Al	1.3079	1.2804	1.2320	1.2382	1.0304	1.3062
Ca	0.3015	0.2697	0.2337	0.2415	0.0185	0.2966
Na	0.6917	0.6724	0.7029	0.7299	0.8958	0.6374
K	0.0180	0.0171	0.0174	0.0163	0.0081	0.0078
O site	1.0112	0.9592	0.9540	0.9877	0.9224	0.9418
T site	3.9923	4.0127	4.0109	3.9975	4.0223	4.0168

oxide weight percent in all samples. Generally, the higher iron values occur in the biotite quartz diorite and the lowest values in the porphyritic core phase.

Magnetite

Analyzed magnetite grains contain iron, minor amounts of titanium and aluminum, and trace amounts of calcium, magnesium, manganese, and chromium. No evidence of ilmenite exsolution was observed under reflected light microscope or under scanning electron beam imaging. The minor concentrations of titanium and aluminum may represent limited ilmenite and hercynite solid solutions. In the absence of coexisting iron oxide pairs that would provide simultaneously determinations of temperature and oxygen fugacity, no further work was done on magnetite.

CHAPTER 5

THERMODYNAMIC SOLUTION MODELS

Currently there are three different thermodynamic solution models for the dehydration reaction of annite to form alkali feldspar, magnetite, and water:

(1) an ideal solution model presented by Czamanske and Wones (1973) for the dehydration reaction along the annite-phlogopite join;

(2) an ideal solution model presented by Partin (1984, 1983) for the dehydration reaction along the annite-oxyannite join; and

(3) an athermal solution model presented by Beane (1974, 1972) for the dehydration in the ternary system annite-phlogopite-oxyannite.

Each of these models is briefly reviewed below.

An Ideal Solution Model

Wones and Eugster (1965) outlined a binary regular solution model for the stability of biotites at magmatic temperature and pressure and various oxygen fugacities. Based on their experimental work (Eugster and Wones, 1962; Wones, 1963) Eugster and Wones suggested that the mixing of

annite and phlogopite followed a regular solution model:

(5.1) $\log \delta_i = (1 - X_i^2)^2 \, W / 2.303 \, RT$

(Wones and Eugster, 1965). In Equation (5.1) δ_i and X_i refer to the activity coefficient and the molecular proportion of Fe^{2+} in biotite, respectively, and W is a regular solution interaction parameter.

Mueller (1972) commented that the biotite compositions treated by Eugster and Wones belonged to the ternary system annite-phlogopite-oxyannite, and by considering the system to be pseudo-binary they produced large activity coefficients along the annite-phlogopite join. Mueller observed that in natural assemblages the Fe-Mg exchange between co-existing ferromagnesian silicates was largely ideal; and therefore, inconsistent with large activity coefficients along that join (Mueller, 1972). He proposed an ideal solution model for the Fe^{2+}-Mg exchange between the end- member biotites. Mueller (1972) defined the activity of annite as one-third of a formula unit of biotite:

(5.2) $\alpha Fe^{bi} = XFe^{bi} \, \delta Fe^{bi}$

where Fe represents the annite component in biotite and α, X, and δ refer to the activity, the mole fraction, and the activity coefficient, respectively. In a reply to Mueller's comments Wones (1972) agreed that Mueller's definition of the activity of annite was correct and that the ideal solution model was supported by their own later experimental

work (Wones, Burns, and Carroll, 1971; Huebner and Sato, 1970; Wones and Gilbert, 1969).

In 1973, Czamanske and Wones applied the revised 1972 solid solution model to a natural system, the Finnmarka complex in Norway (Czamanske and Wones, 1973). At Finnmarka the biotites are fluorine-rich; therefore, the biotite solid solution model was further modified to account for the increased stability of fluorine-rich biotites. Following the ionic solution model, the activity of annite was define as:

(5.3) $\alpha annite = (XFe^{2+})^3(XOH)^2$

where α and X represent activity and site fraction, respectively (Czamanske and Wones, 1973). They assumed that the exchange of F and OH in hydroxyl site was ideal.

An Ideal Solution Model for the Annite-Oxyannite Join

Partin (1983, 1984) has completed the most recent experimental work on solid solution along the annite-oxyannite join. She has found that the Fe^{3+} substitution for Fe^{2+} occurs by the oxyannite mechanism:

(5.4) $Fe^{3+} + O^{2-} = Fe^{2+} + OH^-$

and the creation of interlayer vacancies:

(5.5) $Fe^{3+} + []_i = Fe^{2+} + R^+_i$

where R^+_i represents a monovalent interlayer cation (K^+ or Na^+) and $[]_i$ represents a vacancy in the interlayer (Hewitt

and Wones, 1984). Partin used her data to modify the equilibrium constant of Czamanske and Wones (1973). The resulting formulation for the activity of annite is the same as that defined by Czamanske and Wones (1973) (Hewitt and Wones, 1984).

Partin's model of ideal mixing of the Fe^{3+} and Fe^{2+} components is in disagreement with the theoretical evaluation by Mueller and Saxena (1977) of the exchange between cations with non-equivalent valence in a silicate lattice.

An Athermal Solution Model

In 1972, Beane proposed a parabolic-athermal solution model for biotite compositions within the phlogopite-annite-oxyannite ternary system based on experimentally determined free energy of mixing terms. The activity of annite takes on the form:

(5.6) $\alpha ann = Xann\ \delta ann.$

Note that in this model the activity of annite does not follow the ionic formulation used by Wones and Eugster (1965), Mueller (1972), Wones (1972), or Czamanske and Wones (1973). In Beane's parabolic-athermal model the activity of annite is proportional to the molecular proportion of annite in the ternary phase. Beane further requires that the sum of the molecular proportions of the ternary components equals one:

(5.7) $Xann + Xphl + Xoxy = 1.$

Within Beane's parabolic athermal model, the highest degree of ideality occurs along the annite-phlogopite join which is in agreement with the experimental work of Wones and others (Wones, Burns, and Carroll, 1971; Huebner and Sato, 1970; Wones and Gilbert, 1969) and Mueller's analysis of coexisting biotites and other ferromagnesian silicates in natural systems (Mueller, 1972). The greatest departure from ideality occurs along the annite-oxyannite join. The extent of non-ideality is reflected in Beane's solution model by the large negative Margules parameters for the annite-oxyannite pair (Beane, 1974).

A criticism of Beane's model stems from whether an athermal mixing model should be applied to a silicate solid solutions (Ganguly and Saxena, in press). Traditionally, athermal mixing models have been applied to solutions of large organic polymers that have a large difference in the absolute size, weight, and geometry between the solute and solvent molecules. These solutions show large deviations from Raoult's Law at low concentrations, yet have excess enthalpy of mixing terms that too small to account for the departure form ideality (Prigogine and Defay, 1951). A large excess entropy of mixing term accounts for the non-ideality (Prigogine and Defay, 1951).

If an athermal mixing model is to be applied to the annite-oxyannite solid solution one would have to demonstrate that the excess enthalpy of mixing is too small to

account for the non-ideality and that mixing units of annite and oxyannite are significantly different in size, shape, or molecular weight. If one compares the lattice dimensions of annite and oxyannite as well as their molecular weights one finds that there is not more than a few percent difference. In addition, an excess enthalpy of mixing term that is zero or very small implies that the Fe^{2+}, Mg^{2+}, and Fe^{3+} cations react with the silicate lattice in an energetically equivalent way. However, the interactions of divalent and trivalent cations with the silicate lattices are not likely to be equivalent (Saxena, 1973; Mueller and Saxena, 1977).

Discussion

The choice of the biotite solution model determines the formulation of the activity of the annite component that is substituted into Equation 5.8:

(5.8) $\log K_{eq} = \log fH_2O - \log \alpha ann - 1/2 \log fO_2$.

The biotites in this study contain a significant mole fraction of oxyannite component; therefore, it is important to consider whether the oxyannite component will affect the ideality of mixing between the annite and phlogopite end members. I have evaluated the sensitivity of the activity of annite to the mole fraction of oxyannite component by adopting a regular ternary solution model, with an ionic formulation for the activity of the annite

component, and by further assuming that the Fe-Mg exchange between annite and phlogopite end members is ideal.

If the standard state for the biotite dehydration reaction is chosen as pure solid phases at pressure and temperature of interest and pure gases at one bar pressure and temperature of interest, then the equilibrium constant for the reaction is represented by Equation 5.8. By the definition of an ionic solution model, the activity of annite is represented by:

(5.9) $\alpha ann = (XFe^{2+})^3 (XOH)^2 \delta ann$

where $XFe^{2+} = Fe^{2+}/6$ and δann is the activity coefficient for the annite component. The activity coefficient can be broken into the partial components δFe^{2+} and δOH (Saxena, 1973). Collecting the mole fraction and partial activity coefficient terms, the activity of annite becomes:

(5.10) $\alpha ann = (XFe^{2+})^3 (XOH)^2 \delta ann$

For a ternary regular solution model the partial activity coefficients have the form:

(5.11) $RT \ln\delta_i = W_{ij} X_j^2 + W_{ik} X_k^2 + \{W_{ij} + W_{ik} - W_{jk} - C(1 - 2X_i)\} X_j X_k$

where W and X are the Margules parameters for the binary system of subscripted phases and site fraction of the subscripted ternary phases i, j, and k, respectively, and C is the ternary interaction coefficient (Ganguly and Saxena, in press). If i = annite, j = phlogopite, and k = oxyannite then Equation 5.11 becomes:

(5.12) $RT \ln\delta_a = W_{ap}X_p^2 + W_{ao}X_o^2 + \{W_{ap} + W_{ao} - W_{po} - C(1 - 2X_a)\}X_pX_o$

where the subscripts a, p, and o refer to annite, phlogopite, and oxyannite, respectively. The first term vanishes because the substitution along the annite-phlogopite join is assumed ideal: $W_{ap} = 0$. The site fraction of oxyannite is small, between 0.05 and 0.1; therefore, the second term, $W_{ao}X_o^2$, should be very small. Evaluating the third term is more complex: $W_{ap} = 0$, and W_{ao} and W_{po} should be of roughly the same magnitude and cancel out if the energetics of reaction between the annite-oxyannite and phlogopite-oxyannite end members are similar. The magnitude of the ternary interaction coefficient, C, is not known; however, the contribution of the remaining part of the third term can be estimated. X_a has values between 0.3 and 0.4; therefore, the quantity $1 - 2X_a$ will be between 0.2 and 0.4. Values for X_p vary between 0.4 and 0.5, and values for X_o between 0.05 and 0.1. The product $(1 - 2X_a)X_pX_o$ will be a very small number. In this intuitive way it can be seen that even the maximum oxyannite site fraction of 0.1 will not force the annite-phlogopite solid solution from ideality.

Note that the above argument can not be applied to Beane's parabolic-athermal solution model because the formulation of the activity of annite is different:

(5.13) $RT \ln\delta_a = W_{ap}X_{p2} + W_{ao}X_o^2 + (W_{ap} + W_{ao} - W_{po})X_pX_o$.

And the requirement that the sum of the molecular components equals one (see Equation 5.8), greatly increases the effective site fraction of the oxyannite component. Therefore, even a small oxyannite component would have a large influence on the activity coefficient of annite in Equation 5.13.

CHAPTER 6

DETERMINATION OF INTENSIVE VARIABLES

Procedure

The variation in oxygen fugacity during crystallization is estimated using the following biotite dehydration reaction:

(6.1) $KFe_3AlSi_3O_{10}(OH)_2 + 1/2\ O_2 = KAlSi_3O_8 + Fe_3O_4 + H_2O$

The corresponding equilibrium constant is defined:

(6.2) $$\ln K_{eq} = \frac{\alpha KAlSi_3O_8\ \alpha Fe_3O_4\ fH_2O}{\alpha Kfe_3AlSi_3O_8\ fO_2^{1/2}}$$

for a standard state of pure solid phases at pressure and temperature of interest and pure gas phase at 1 bar pressure and temperature of interest. Solving Equation 6.2 for fugacity of oxygen:

(6.3) $$-1/2 \log fO2 = (7409/T) + 4.25 - \log fH2O + \log \alpha annite - \log \alpha KAlSi_3O_8 - \log \alpha Fe_3O_4$$

where T is temperature in degrees Kelvin, and $\alpha KAlSi_3O_8$ and αFe_3O_4 represent the activity of orthoclase in alkali feldspar and the activity of magnetite in Fe-spinel, respectively. The equilibrium constant for the above reaction was defined by Eugster and Wones (1962) as pure, solid phases at temperature of interest and pressure equal

to 2070 bar and pure gas phases at temperature of interest and 1 bar pressure. Since the change in volume of the solid phases in the above reaction is small, the above equilibrium is relatively insensitive to pressure and no pressure term is required for pressures near 2000 bars.

Activity of Annite

Czamanske and Wones (1973) defined the activity of annite as:

(6.4) $\alpha annite = (XFe^{2+})^3(XOH)^2$

where XFe^{2+} represents the site fraction of ferrous iron in the octahedral layer and XOH represents the site fraction of hydroxyl ion in the hydroxyl site. The mole fraction of ferrous iron was determined by a combination of microprobe data and Mossbauer analysis. In this study the site fraction of ferrous iron in the octahedral is defined as the molecular proportion of ferrous in the octahedral layer divided by 6, the total number of available sites in the octahedral layer. Defining the site fraction in this way, a vacancy in the octahedral layer is counted explictly exchangeable component.

The site fraction of OH^- in the hydroxyl layer is assumed to equal the remaining vacancy in the hydroxyl site after subtracting the ionic proportions of fluorine and chlorine from one:

(6.5) $XOH = 1 - (XF + XCl)$

where XF and XCl are determined by microprobe analysis.

Fugacity of Water

The fugacity of H_2O is estimated by two methods:

(1) the crystallization sequence of ferromagnesian phases, as inferred from textural evidence, that are dependent on the partial pressure of water (Naney, 1983);

(2) normalized whole-rock analyses on quartz-albite-orthoclase ternaries contoured for temperature (Tuttle and Bowen, 1958; Luth, et al., 1964; James and Hamilton, 1968; Luth, 1976).

The phase equilibria of ferromagnesian silicates in vapor-unsaturated granitic systems at 2 and 8 kbar has been experimentally determined by Naney (1983). At a constant total pressure the water content of the melt has a significant effect on the order of crystallization of the rock-forming minerals. Based on pressure estimates from stratigraphic reconstruction (Mauger, 1966) I have chosen to compare the petrographic relations observed in the Ruby Star samples to Naney's experimental work at 2 kbar.

(1) The crystallization sequence of the biotite quartz diorite was initial plagioclase with contemporaneous clino-pyroxene followed by biotite and later alkali feldspar and quartz. This sequence suggests that the melt had a water content of about 3.5 weight percent at a total pressure of 2 kbar (Naney, 1983). If equilibrium had been attained

the clinopyroxene would be completely resorbed. The biotite replacement textures of clinopyroxene are consistent with the predicted instability of clinopyroxene.

(2) The crystallization sequence of the hornblende-bearing equigranular granodiorite phase was plagioclase, hornblende, biotite, alkali feldspar and quartz. The crystallization of hornblende required a minimum water content of 4.5 weight percent at 2 kbar (Naney, 1983). Under equilibrium crystallization the hornblende would be completely resorbed.

(3) The crystallization sequence of the porphyritic granodiorite is essentially indistinguishable from the sequence described above for the hornblende-bearing equigranular granodiorite.

The above estimates of water content in the granodiorite represent minimum values since there would be no change in the crystallization sequence if the melt were saturated with respect to water (Naney, 1983).

The normative whole rock compositions are plotted on a quartz-albite-orthoclase-anorthite projection in Figure 12. On an anorthite-albite-orthoclase ternary the samples trace a line from anorthite-rich bulk compositions to orthoclase-rich bulk compositions from the biotite quartz diorite to the porphyritic granodiorite.

If the projections considered to represent portions of the quinary haplogranodiorite system albite-anorthite-

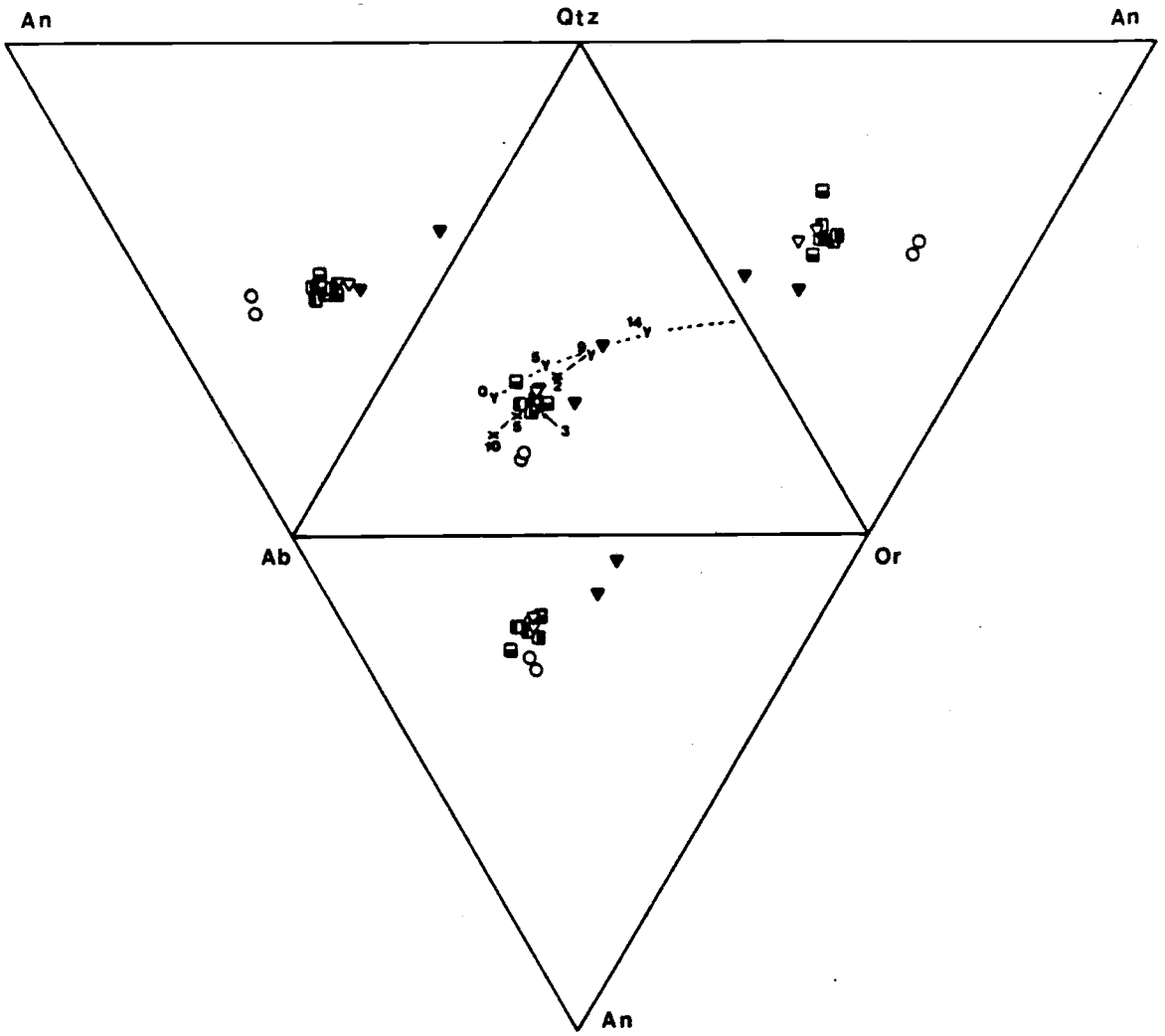

Figure 12. Quartz-Albite-Orthoclase-Anorthite Projection.

Projected normative values on quartz-albite-orthoclase-anorthite quaternary. Ternary eutectics for 2, 3, 5, and 10 kbar are from Tuttle and Bowen (1955) and the eutectics for anorthite contents of 0, 9, and 14 at 5 kbar are from Winkler (1976). The samples cluster at the ternary eutectic for a vapour saturated system at 2 to 3 kbar and 685 C.

orthoclase-quartz-H_2O summarized by Luth (1976), then an estimation of the partial pressure of water and the eutectic temperature can be made. The samples cluster about the eutectic composition for the quaternary system at approximately 2 kbar and at 685 C defined by Tuttle and Bowen (1958). This pressure-temperature pair is a maximum estimate since P_{H_2O} may be less than total pressure.

Activity of Orthoclase

Czamanske and Wones (1973) and Czamanske and others (1981) have adopted the formulation proposed by Waldbaum and Thompson (1969) for the activity of alkali feldspar in igneous rock. Waldbaum and Thompson determined that if the alkali feldspar contains from 0.25 and 0.75 mole percent $KAlSi_3O_8$ and the rock crystallized between 600 and 800 C, then the activity of orthoclase in alkali feldspar is approximately 0.6.

Activity of Magnetite

Since magnetite is ubiquitous in all members of the suite and microprobe analysis of the magnetite indicate that it is relatively pure, the activity of magnetite is assumed to be equal to one for all members of the suite.

Temperature

The determination of oxygen fugacity in Equation 6.2 is most sensitive to the estimates of temperature.

Therefore, estimation of the eutectic temperature for each member of the magmatic suite was attempted by three different methods:

(1) two-feldspar thermometry, using the models of Whitney and Stormer (1977) and Ghiorso (1984),

(2) F-OH exchange equilibrium between coexisting apatite-biotite pairs as defined by Ludington (1978), and

(3) eutectic temperature estimates using normalized whole-rock data plotted on Ab-An-Or ternaries.

Both the Stormer and Whitney (1977) two-feldspar thermometer and the Ghiorso (1984) two-feldspar thermometer produce eutectic temperatures between 500 C and 600 C for the Granodiorite (see Table 6). This temperature range is about 100 degrees cooler than the eutectic temperatures experimentally determined by Wyllie (1981) for granites with a bulk composition similar to the Ruby Star Granodiorite at vapor saturation and 2000 bars. The low two-feldspar "eutectic" temperatures suggest that the Ruby Star Granodiorite may have partially re-equilibrated with hot deuteric water after crystallization.

The fluorine-hydroxyl exchange thermometer was first proposed by Stormer and Carmichael (1971). It was later modified by Duff (1971) and Ludington and Munoz (1975) to include new thermodynamic data on apatite and additional information on F-OH exchange in biotites. Ludington (1978) used these data and introduced the following formulation:

Table 6
Estimates of Eutectic Temperature (C)

	Equigranular Rim East RS MR 5	Equigranular Rim West RS MR 8	South RS MR3 6	South RS SM 1	Porphyry Core RS MR3 8	Aplite Dike RS MR 4	Biotite Diorite DMR2 3
Whitney and Stormer (1977)							
high	491	518	498	509	541	462	563
average	485	511	491	463	509	448	554
low	479	495	454	456	483	437	535
Ghiorso (1984)							
high	565	570	497	565	571	495	616
average	527	547	495	500	554	460	602
low	498	498	425	427	536	425	585
Ludington (1978)							
high	861			649			
average	659			643			
low	485			606			

Table 7
Fluorine and Chlorine Analyses of Biotite and Apatite

	Equigranular Rim East RS MR 5	Equigranular Rim West RS MR 8	South RS SM 1	Porphyry Core RS MR3 8	Aplite Dike RS MR 6
Apatites					
F	1.0159	1.3012	0.9071	1.1378	1.2175
Cl	0.0043	0.0028	0.0072	0.0014	0.0592
Biotites					
F	0.1428	0.2221	0.2984	0.4438	0.358
Cl	0.0051	0.0076	0.0127	0.0101	0.0101

(6.6) $T(K) = 1000/\log [Xf/Xoh]_{ap} + \log [Xoh/Xf]_{bio} - 1.107Xann - 1.444Xsid.$

Only apatites that were enclosed in biotite were analyzed in attempt to minimize complications resulting from resetting of F-OH partitioning by post-magmatic fluids and possible difficulties involving differential exchange kinetics. Fluorine and chlorine microprobe analyses of the biotite-apatite pairs are listed in Table 7. Only three of the twenty apatites analyzed contain stoichiometric amounts of fluorine; the remainder contained between 1.0159 and 1.3012 mole fraction fluorine. Temperatures produced by the fluorine-hydroxyl exchange thermometer are much higher than the temperatures predicted by either feldspar model (see Table 6).

The temperatures calculated by the three thermometers suggest that entire batholith crystallized within a 75 C interval. Since the error in the two-feldspar model is +/- 60 C it is not possible to resolve the sequence in which the members of the Granodiorite crystallized.

The eutectic temperature indicated by the Tuttle and Bowen ternary for the Granodiorite is 685 C at 2000 to 3000 bars and vapor saturation (Figure 12). This temperature is about 100 higher than temperatures calculated by two-feldspar thermometry and falls within the range of eutectic temperatures found by Wyllie (1981).

Results: Calculation of Oxygen Fugacity

Substituting the values for activity of annite for the equigranular rim and the porphyritic core into Equation 6.3 generates the traces of the upper limit of biotite stability in temperature-fO_2 space shown in Figure 13. The trace of the upper limit of biotite stability indicates that the Ruby Star Batholith crystallized under conditions of high oxygen fugacity. A trace of the crystallization path through temperature-fO_2 space cannot be drawn because attempts to resolve the temperature of crystallization for each member of the Granodiorite have failed.

A trend of increasing oxygen fugacity is suggested by Figure 6 which shows the decreasing Fe/(Fe + Mg) content of biotite and the increasing Fe/(Fe + Mg) content of the host rock plotted against the SiO_2 content of the host rock. Murakami (1969) interpreted the trend of Mg-enrichment in biotite with simultaneous Fe-enrichment in the host rock as indicating a progressively more oxidizing environment (Speer, 1984).

Many authors have suggested that the ferrous silicates may buffer the oxygen fugacity during crystallization (Osborn, 1962). The buffering effect of ferrous silicates is observed in the Bushveld Complex and other more mafic intrusive suites. Mueller has used mass balance equations to demonstrate that the abundance of ferrous silicates is not sufficient to buffer the oxygen fugacity in

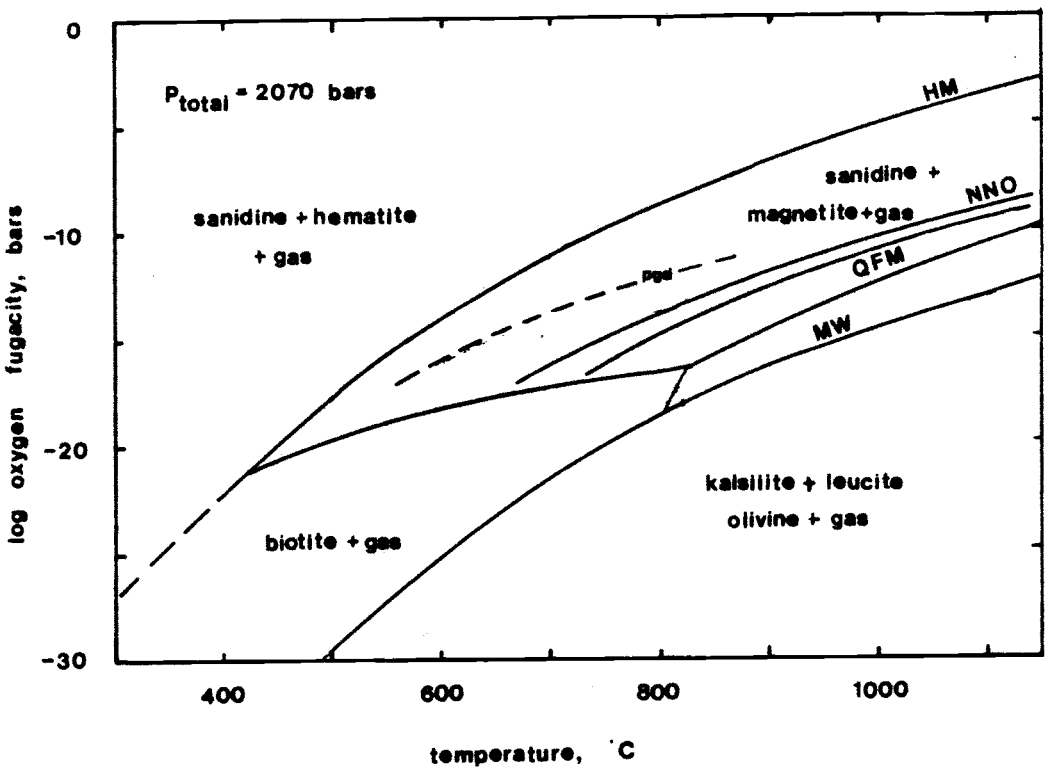

Figure 13. Stability of Ruby Star Biotite.

The light dashed line represents the upper limit of stability of biotite from the porphyritic granodiorite (pgd) in fO_2 - temperature space. The light solid lines are buffers: HM, hematite - magnetite; NNO, Ni - NiO; QFM, quartz - fayalite - magnetite; MW, magnetite - wustite. After Eugster and Wones, 1965.

rocks of granodiorite composition (Mueller, 1969). The most prescribed mechanism to buffer oxygen fugacity during crystallization is the coexistence of separate water-rich fluid that acts as the oxidizing medium through dissociation of water and hydrogen loss (Speer, 1984; De Pieri and Jobstraibizer, 1983).

Intrusive suites that contain biotites with a uniform $Fe^{2+}/(Fe^{2+} + Mg)$ ratio, such as the Ruby Star, have been interpreted as reflecting re-equilibration with deuteric fluids (Speer, 1984; Dodge and Moore, 1968). If the Fe and Mg content of the biotite reflect re-equilibration then the composition of the hydroxyl site in biotite should also re-equilibrate with deuteric fluids (Munoz, 1984). As Figure 9, shows the Granodiorite biotite fluorine and chlorine intercept values plot in the field of primary igneous biotite. Therefore, I believe that the limited variation in the Fe/(Fe + Mg) ratio of the biotite does not represent re-equilibration, but rather reflects the uniform bulk composition of the Granodiorite.

CHAPTER 7

COMPARISON TO OTHER STUDIES

Many other studies have used the variation in the chemistry of biotite and hornblende as a means of estimating the variation of intensive variables during the crystallization of felsic magmatic suites. Before comparing the results of this study to other studies, it is informative to evaluate the sensitivity of the biotite dehydration reaction on its dependent variables.

Sensitivity

The sensitivity of oxygen fugacity on its dependent variables is outlined in Table 8. As the numeric value of any variable increases it causes a corresponding increase in oxygen fugacity. Oxygen fugacity is most sensitive to the estimate of temperature. The fugacity of water is the next most significant variable. Most of the variation in the estimated values of oxygen fugacity from study to study is created by the chosen formulation of the activity of annite and magnetite. As the activity coefficients of biotite and magnetite are assumed to be one in all the studies, the oxygen fugacity is directly dependent on the on the calcu-

Table 8

Sensitivity of Oxygen Fugacity

to Dependent Variables

Variable (X)	Change in variable (ΔX)	Resultant change in oxygen fugacity
temperature	50 C	0.7 log units
pressure	1000 bars	0.6 log units
activity of annite	XFe = 0.1	0.23 log units
	XOH = 0.1	0.1 log unit
activity of orthoclase	$\alpha KAlSi_3O_8$ = 0.1	0.1 log unit
activity of magnetite	αFe_3O_4	0.1 log unit

Table 9

Assumptions Compared

Study Area	Estimated T(C)	Estimated P(bars)	Activity of annite	Activity of orthoclase	Activity of magnetite
Cartridge Pass	650 - 900	1000	$\frac{Fe}{Fe + Mg}$	1	1
Central Nevada Batholith	700 - 800	1000 - 2000	XFe	$XKAlSi_3O_8$	1
Aregos Complex	680 - 800	2000 - 3000	$\frac{Fe}{Fe + Mg}$	1	1
Finnmarka	625 - 725	1000	XFe^3XOH^2	0.6	1
Ploumanc'h Complex	550	800 - 1000	XFe^3	0.85	0.95

lation of the annite component in biotite and the magnetite component in the Fe-spinel.

Other Studies

The following studies have attempted a similar evaluation of oxygen fugacity during crystallization of magmatic suites using biotite compositions as an indicator:

Dodge and Moore (1968)	Cartridge Pass, Sierra Nevada
Dodge, Smith and May (1969)	Central Nevada Batholith
Czamanske and Wones (1973)	Finnmarka Complex, Norway
de Albuquerque (1973)	Aregos Complex, Portugal
Barriere and Cotten (1979)	Ploumanac'h Complex

Figure 14.1 is a plot in temperature-oxygen fugacity space showing the distribution of conditions of crystallization as indicated by the authors. The crystallization path of the Finnmarka Complex (Czamanske and Wones, 1973) shows the greatest increase in oxygen fugacity with decreasing temperature. The Cartridge Pass Pluton (Dodge and Moore, 1968) has the highest temperature-oxygen fugacity conditions during crystallization, though the authors believe that the uniform composition of biotites indicates that the biotites had re-equilibrated with late stage fluids. The Central Sierra Nevada Batholith (Dodge and others, 1969) crystallized under the most reduced conditions.

Although all the above studies use the biotite dehydration reaction (Equation 6.1) as proposed by Eugster

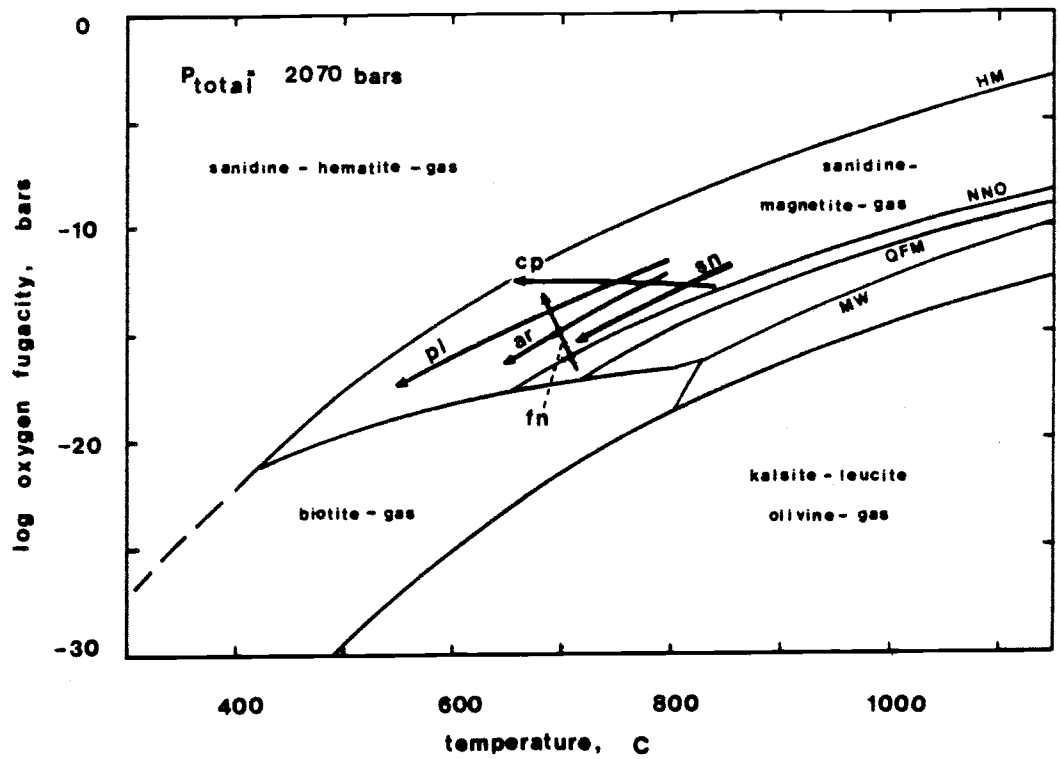

cp - Cartridge Pass Pluton
sn - Sierra Nevada Batholith
pl - Ploumanac'h Igneous Complex
ar - Aregos Granitoids
fn - Finnmarka Complex

Figure 14.1. Stability of Biotites From Other Granodiorites.

The bold arrows represent traces of the crystallization paths of intrusive suites of granodiorite composition through fO_2 - temperature space as calculated by the authors: Aregos granitoids, Portugal (de Albuquerque, 1973), Sierra Nevada Batholith, California (Dodge et al., 1969), Ploumanac'h igneous complex, France (Barriere and Cotten, 1979), Finnmarka complex, Norway (Czamanske and Wones, 1973), and the Cartridge Pass pluton, California (Dodge and Moore, 1968). The light lines are the buffers as indicated in Figure 11. After Speer (1984).

and Wones (1965) or the modified version of Czamanske and Wones (1973) the assumptions made in applying the equilibrium vary widely. The plutons studied, together with the estimated pressure and temperature of crystallization, and the activities of annite, alkali feldspar, and magnetite are listed in Table 9. In order to compare the plutons on a uniform basis I have used the authors' estimates of pressure and temperature of crystallization, but I have used Equation 3.5 to calculate the activity of annite and used Waldbaum and Thompson's formulation for the activity of alkali feldspar. Figure 14.2 is a plot of the revised temperature-oxygen fugacity conditions during crystallization of granodiorite from the various study areas.

In Figure 14.2 the granodiorite suites appear to have crystallized in more limited range of temperature - fO_2 conditions and generally at lower oxygen fugacities than those suggested by the authors. Also note that the Ruby Star Granodiorite crystallized at higher fO_2 - temperature conditions than most of the other granodiorite suites. The Finnmarka complex is the obvious exception. The Fe/(Fe + Mg) content of biotites from Finnmarka have the decrease from 0.64 to 0.26 with increasing silica content of the host rock (Czamanske and Wones, 1977); therefore, the positive slope of the crystallization path in Figures 14.1 and 14.2 is valid. However, the steepness of the crystallization path results largely from the assumption that crystalli-

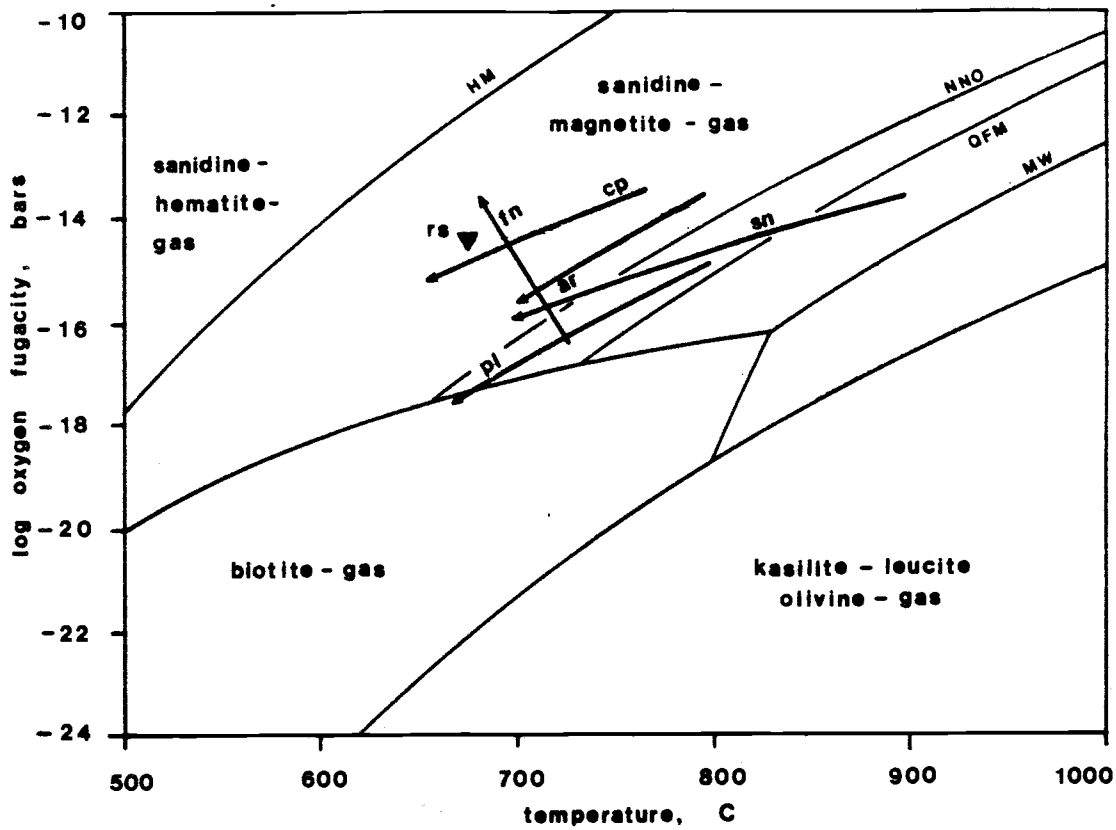

rs - Ruby Star Granodiorite
cp - Cartridge Pass Pluton
sn - Sierra Nevada Batholith
pl - Ploumanac'h Igneous Complex
ar - Aregos Granitoids
fn - Finnmarka Complex

Figure 14.2. Recalculated Stability of Biotites from Other Granodiorites.

The traces of the crystallization path through fO_2 - temperature for the granodiorites in Figure 19.1 have been recalculated using the assumptions in Table 9. The resulting traces are shown here. Biotites from the Ruby Star Granodiorite are represented by the solid triangle.

zation occurred during a temperature decrease of only 40 C (Czamanske and Wones, 1973). The trace of the Cartridge Pass pluton intersects the temperature-fO_2 conditions of crystallization of the Ruby Star Granodiorite. Dodge and Moore (1968) believed that the uniform Fe/(Fe + Mg) content of the Cartridge Pass biotites represents re-equilibration with late stage fluids. Although the biotites from the Ruby Star Granodiorite also show little variation in their Fe/(Fe + Mg) content I do not believe that the biotite compositions are the result of re-equilibration for the following reasons: (1) the Fe/(Fe + Mg) content shows a systematic variation with SiO_2 content of the host rock (Figure 6), and (2) the composition of the hydroxyl site has primary igneous character (Figure 9).

Possible Implications to Porphyry Copper Mineralization

The range in temperature and fO_2 conditions during crystallization of the Ruby Star batholith match exactly with the temperature and fO_2 conditions predicted by Burnham and Ohmoto (1980) for porphyry copper and porphyry gold deposits (see Figure 15). Burnham and Ohmoto based their calculations on the temperature and fO_2 conditions required for a hydrothermal fluid to carry the appropriate sulfur species for copper complexing. However, Burnham predicted that the fO_2 would decrease during the crystallization of the

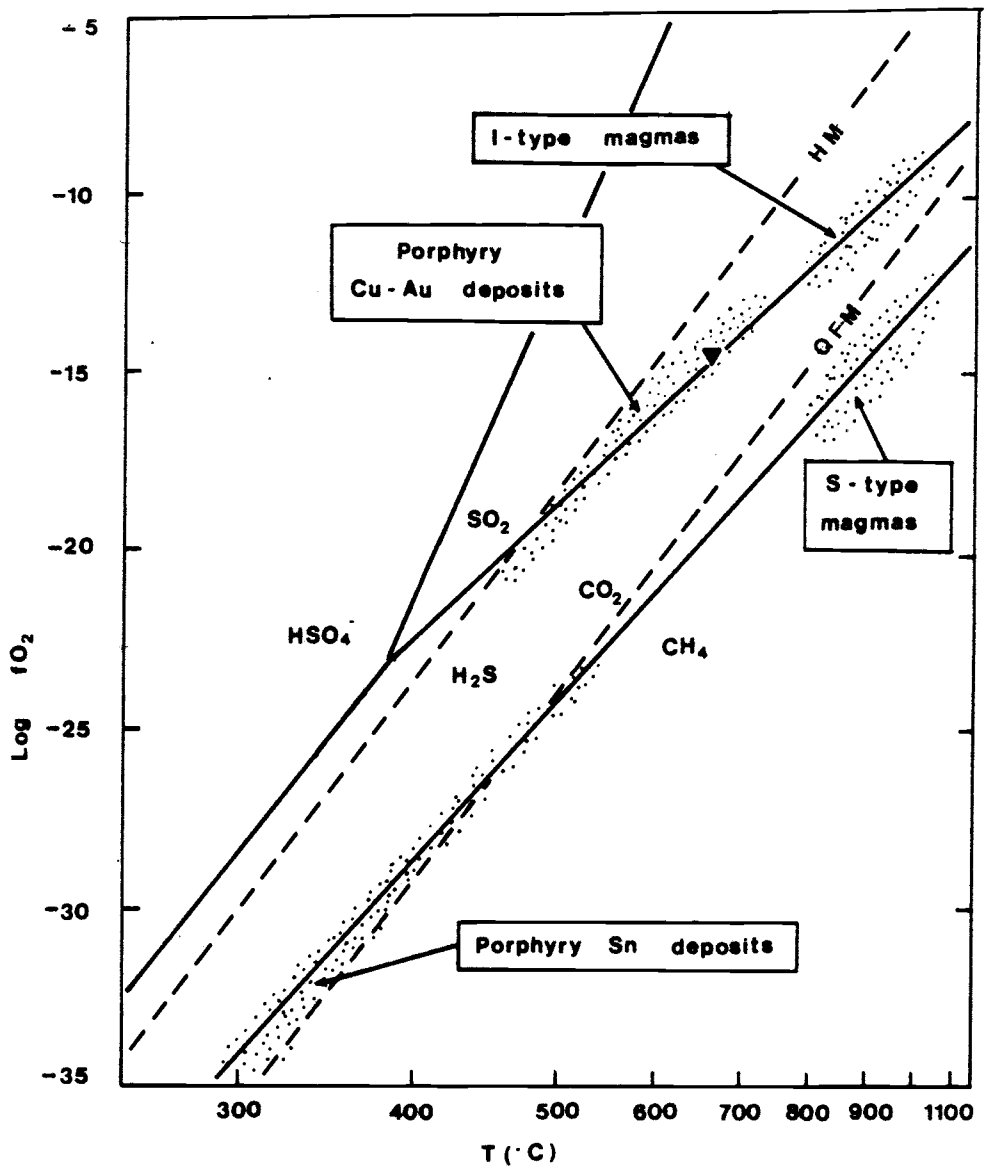

Figure 15. Predicted fO_2-T Conditions for Porphyry Mineralization.

The stippled areas represent the predicted fO_2-temperature conditions for various types of porphyry mineralization (Burnham and Ohmoto, 1980). The solid triangle, representing the Ruby Star biotites, plots in the region appropriate for porphyry copper deposits. The solid lines are phase boundaries for the sulfur and carbon species. The dashed lines represent the hematite-magnetite and the quartz-magnetite-fayalite buffers.

porphyry host. The Ruby Star granodiorite shows an slightly oxidizing trend. This correlation may suggest that Burnham and Ohmoto are correct in their theory that a potential porphyry host must eventually fall within the predicted range of fO_2 and temperature conditions if mineralization is to occur but the path of evolution of oxygen fugacity may not be critical to porphyry copper mineralization.

In conclusion, the temperature, fH_2O, and fO_2 conditions of crystallization of a porphyry copper host can be determined using thermodynamic solid solution models for ferromagnesian silicates. In this study it was found that the oxygen fugacity during crystallization was high compared to the granodiorites of other studies and met the values predicted by Burnham and Ohmoto (1980). Chivas' study (Chivas, 1981; Hendry et al., 1981) on intrusive suites associated with a porphyry copper occurrences also found that crystallization took place under progressively more oxidizing conditions. Only similar studies of other porphyry copper deposits will confirm whether an oxidizing trend is significant in the porphyry copper mineralization process.

REFERENCES

Anthony, E.Y., 1986, Geochemical evidence for crustal melting at the Sierrita porphyry copper deposit, Southeastern Arizona: PhD Dissertation, University of Arizona, Tucson.

Barker, D.S., 1983, Igneous Rocks, Prentice-Hall, Inc., Englewood Cliffs, New Jersey, 417p.

Barriere, M. and Cotten, J., 1979, Biotites and associated minerals as markers of magmatic fractionation and deuteric equilibration in granites: Contributions to Mineralogy and Petrology, vol. 78, pp. 182-192.

Beane, R., 1974, Biotite stability in porphyry copper environments: Economic Geology, vol. 69, pp. 241-256.

Beane, R.E., 1972, A thermodynamic analysis of the effect of solid solution on the hydrothermal stability of biotite: PhD Dissertation, Northwestern University, Evanston, Ill.

Burnham, C.W., Holloway, J.R., and Davis, N.F., 1969, Thermodynamic properties of water at 1000 C and 10,000 bars: Geological Survey of America Special Paper 132, 96p.

Burnham, C.W. and Ohmoto, H, 1980, Late stage processes of felsic magmatism: Mining Geology Special Issue, No. 8, pp. 1-11.

Chivas, A.R., 1981, Geochemical evidence for magmatic fluids in porphyry copper mineralization: Contributions to Mineralogy and Petrology, vol. 78, pp. 389-403.

Cooper, J.R., 1960, Some geologic features of the Pima Mining District, Pima County, Arizona: U.S. Geological Survey Bulletin No. 1112-C, pp. 63-103.

Cooper, J.R., 1971, Mesozoic stratigraphy of the Sierrita Mountains, Pima County, Arizona: U.S. Geological Survey Professional Paper No. 658-D, pp. D1-42.

Cooper, J.R., 1973, Geologic map of the Twin Buttes Quadrangle, southwest of Tucson, Arizona: U.S. Geological Survey Misc. Geol. Inv. Map I-745.

Czamanske, G.K., Ishihara, S., Aiken, S.A., 1981, Chemistry of Rock-forming minerals of the Cretaceous-Paleocene batholith in Southwestern Japan and implications for magma genesis: Journal of Geophysical Research, vol. 86, no. B11, pp. 10431-10469.

Czamanske, G.K. and Wones, D.R., 1973, Oxidation during magmatic differentiation, Finnmarka Complex, Oslo area, Norway: Part 2, the mafic silicates, Journal of Petrology, vol. 14, part 3, pp. 349-380.

Damon, P.E., compiler, 1965, Correlation and chronology of ore deposits and volcanic rocks: Tucson, Ariz., Arizona Univ. Geochronology Lab. Ann. Prog. Rept. COO-689-50 to U.S. Atomic Energy Comm.

Damon, P.E., 1966, Correlation and chronology of ore deposits and volcanic rocks: Tucson, Ariz., Arizona Univ. Geochronology Lab. Ann. Prog. Rept. COO-689-60 to U.S. Atomic Energy Comm.

de Albuquerue, C.A.R., 1973, Geochemistry of biotites from granitic rocks, Northern Portugal: Geochimica et Cosmochimica Acta, vol. 37, pp. 1779-1802.

De Pieri, R. and Jobstraibizer, P.G., 1983, Crystal chemistry of biotites from dioritic to granodioritic rock-types of Adamello Massif (Northern Italy): Neues Jahrbuch Miner. Abh., vol. 148, no. 1, pp. 58-82.

Dodge, F.C.W., and Moore, J.G., 1968, Occurrence and composition of biotites from the Cartridge Pass pluton of the Sierra Nevada batholith, California: Geological Survey Professional Paper 600-B, pp. B6-B10.

Dodge, F.C.W., Smith, V.C., and Mays, R.E., 1969, Biotites from granitic rocks of the central Sierra Nevada batholith, California: Journal of Petrology, vol. 10, pp. 250-271.

Duff, E.J., 1971, Orthophosphates, part V: phase equilibria in the system calcium oxide-phosphorous pentoxide-calcium fluoride-water along the fluorapatite-hydroxyapatite join under aqueous conditions: Journal of the Chemical Society, A, pp. 1895-1898.

Eugster, H.P., and Wones, D.R., 1962, Stability relations of the ferruginous biotite, annite: Journal of Petrology, vol. 3, pp. 82-125.

Ghiorso, M.S., 1984, Activity/composition relations in the ternary feldspars: Contributions to Mineralogy and Petrology, vol. 87, pp. 282-296.

Hammarstrom, J.M., and Zen, E-an, 1985, An empirical equation for igneous calcic amphibole geobarometry: Geological Society of America, Abstracts with Programs, vol. 17, no. 7.

Hammarstrom, J.M., and Zen E-an, 1983, Possible use of Al content in hornblende as a geobarometer for plutonic rocks: Geological Society of America, Abstracts with Programs, vol. 15.

Hendry, D.A.F., Chivas, A.R., Reed, S.J.B., Long, J.N.P., 1981, Geochemical Evidence for magmatic fluids in porphyry copper mineralization, part II: Contributions to Mineralogy and Petrology, vol. 78, pp. 404-412.

Hewitt, D.A. and Wones, D.R., 1984, Experimental phase relations of the micas, in, S.W. Bailey, ed., Micas: Reviews in Mineralogy Volume 13, Bookcrafters, Inc., Chelsea, Michigan, pp. 201-247.

Huebner, J.S. and Sato, M., 1970, The oxygen fugacity-temperature relationships of manganese oxide and nickle oxide buffers: American Mineralogist, vol. 55, pp. 934-952.

Irvine, T.N., and Baragar, W.R.A., 1971, A guide to the chemical classification of volcanic rocks: Canadian Journal of Earth Sciences, vol. 8, pp. 523-548.

James, R.S. and Hamilton, D.L., 1969, Phase relations in the system $NaAlSi_3O_8$-$KAlSi_3O_8$-$CaAl_2Si_2O_8$-SiO_2 at 1 kilobar water vapor pressure: Contributions to Mineralogy and Petrology, v. 21, pp. 111-141.

Lovering, T.G., Cooper, J.R., Drewes, H., and Cone, G.C., 1970, Copper in biotite from igneous rocks in southern Arizona as an ore indicator: U.S. Geological Survey Professional Paper No. 700-B, pp. B1-8.

Ludington, S., 1978, The biotite-apatite geothermometer revisited: American Mineralogist, vol. 63, pp. 551-553.

Ludington, S.D., and Munoz, J.L., 1975, Application of fluor-hydroxyl exchange data to natural mica: Geological Society of America, Abstracts with Programs, vol 7, p. 1179.

Luth, W.C., 1976, Part IIB Experimental petrology: igneous rocks, i. granitic rocks, in, D.K. Bailey, ed., The Evolution of the Crystalline Rocks, Academic Press, New York, pp. 333-418.

Luth, W.C., Jahns, R.H., and Tuttle, F.O., 1964, The granite system at pressures of 4 to 10 kilobars: Journal of Geophysical Research, v. 69, no. 4, pp. 759-773.

Mauger, R.L., 1966, A petrographic and geochemical study of the Silver Bell and Pima Mining Districts, Pima County, Arizona: PhD Dissertation, University of Arizona, Tucson.

Mueller, R.F, 1972, Stability of biotite: a discussion: American Mineralogist, vol. 57, pp. 300-316.

Mueller, R.F., 1969, Hydration, oxidation, and the origin of the calc-alkaline series: National Aeronautics & Space Administrations Technical Note D-5400.

Mueller, R.F. and Saxena, S.K., 1977, Chemical Petrology, Springer-Verlag, New York, 394p.

Munoz, J.L., 1984, F-OH and Cl-OH exchange in micas with applications to hydrothermal ore deposits, in, S.W. Bailey, ed., Micas: Reviews in Mineralogy Volume 13, Bookcrafters, Inc., Chelsea, Michigan, pp. 469-491.

Murakami, N., 1969, Two contrastive trends of evolution of biotite in granitic rocks: Ganseki Kobutsu Kosho Gakkaishi (Journal of Japanese Association of Mineralogy, Petrology, and Economic Geology), vol 62, pp. 223-247.

Naney, M.T., 1983, Phase equilibria of rock-forming ferromagnesian silicates in granitic systems: American Journal of Science, vol. 283, pp. 993-1033.

Osborn, E.F., 1962a, Reaction series for subalkaline igneous rocks based on different oxygen pressure conditions: American Mineralogist, vol. 47, pp. 211-226.

Partin, E., 1984, Ferric/ferrous determinations in synthetic biotite. M.S. thesis, Virginia Polytechnical Institute and State University, Blacksburg.

Partin, E., Hewitt, D.A., and Wones, D.R., 1983, Quantification of Fe^{3+} in biotite: Geological Society of America, Abstracts with Programs, vol. 15, pp. 659.

Peters, E.K., Grissom, G.C., Hollister, L.S., and Sisson, V.B., and Stowell, H.H., 1985, Pressure of crystallization of calcalkaline plutons based on aluminum content of hornblende: EOS, vol. 66, no. 18.

Prigogine, I., and Defay, R., 1951, Chemical Thermodynamics, (English translation by D.H. Everett, 1954) Longmans Green, London.

Ransom, F.L., 1922, Ore deposits of the Sierrita Mountains, Pima County, Arizona: U.S. Geological Survey Bulletin No. 725-J, pp. 407-428.

Saxena, S.K., 1973, Thermodynamics of Rock-Forming Crystalline Solutions: Minerals, Rocks and Inorganic Materials, 8, Springer-Verlag, New York.

Speer, J.A., 1984, Micas in igneous rocks, in, S.W. Bailey, ed., Micas: Reviews in Mineralogy Volume 13, Bookcrafters, Inc., Chelsea, Michigan, pp. 299-356.

Stormer, J.C., and Carmichael, I.S.E., 1971, Fluorine-hydroxyl exchange in apatite and biotite: a potential igneous geothermometer: Contributions to Mineralogy and Petrology, vol. 31, pp. 121-131.

Titley, S.R., 1982, Advances in Geology of the Porphyry Copper Deposits, Southwestern North America, S.R. Titley, ed., University of Arizona Press, Tucson, 560 p.

Titley, S.R., 1982, Some features of tectonic history and ore genesis in the Pima Mining District: Pima County, Arizona, in, S.R. Titley, ed., Advances in Geology of the Porphyry Copper Deposits, Southwestern North America, University of Arizona Press, Tucson, pp. 387-406.

Tuttle, O.F. and Bowen, N.L., 1958, Origin of granite in the light of experimental studies in the system $NaAlSi_3O_8$-$KAlSi_3O_8$-SiO_2-H_2O: Geological Society of America, Memoir 74, 153p.

Waldbaum, D.R., and Thompson, J.B., Jr., 1969, Mixing properties of sanidine crystalline solutions, IV: phase diagrams from equations of state: American Mineralogist, vol. 54, pp. 1274-1-98.

West, R.J., and Aiken, D.M., 1982, Geology of the Sierrita-Esperanza Deposit: Pima Mining District, Pima County, Arizona, in, S.R. Titley, ed., Advances in Geology of the Porphyry Copper Deposits, Southwestern North America, University of Arizona Press, Tucson, pp. 387-406.

Whitney, J.A. and Stormer J.C. Jr., 1977, The distribution of $NaAlSi_3O_8$ between coexisting microcline and plagioclase and its effect on geothermomtric calculations: American Mineralogist, vol. 62, pp. 687-691.

Winkler, H.G.F., 1976, Petrogenesis of Metamorphic Rocks, chapter 18: Formation of migmatites, and the origin of granite magmas, Springer-Verlag.

Wones, D.R., 1980, Contributions of crystallography, mineralogy, and petrology to the geology of the Lucerne pluton, Hancock County, Maine: American Mineralogist, vol. 65, pp. 411-437.

Wones, D.R., 1972, Stability of biotite: a reply: American Mineralogist, vol. 57, pp. 316-317.

Wones, D.R., 1963, Phase equilibria of "ferriannite", $KFe^{2+}{}_3Fe^{3+}Si_3O_{10}(OH)_2$: American Journal of Science, vol. 261, pp. 581-596.

Wones, D.R., Burns, R.G., and Carroll, B.M., 1971, Stability and properties of synthetic annite: American Geophysical Union Transactions, v. 52, pp. 369-370.

Wones, D.R. and Dodge, F.C.W., 1977, The stability of phlogopite in the presence of quartz and diopside, in, D.G. Fraser, ed., Thermodynamics in Geology, D. Reidel Publishing Company, Dordrecht, Holland, pp. 229-247.

Wones, D.R. and Eugster, H.P., 1965, Stability of biotite: experiment, theory, and application: American Mineralogist, vol. 50, pp. 1228-1274.

Wones, D.R. and Gilbert, M.C., 1982, Amphiboles in the igneous environment: Reviews in Mineralogy 9B, Mineralogical Society of America, 355-390.

Wyllie, P.J., 1981, Magma sources in the Cordilleran setting: in, W.R. Dickinson and W.D. Payne, eds., Relations of Tectionics to Ore Deposits in the Southern Cordillera, Arizona Geological Society, vol. 14, pp. 39-48.